Synthesis, photophysics and nonlinear optical properties of stilbenoid pyrimidine-based dyes bearing methylenepyran donor groups.

Sylvain Achelle, Jean-Pierre Malval, Stéphane Aloïse, Alberto Barsella, Arnaud Spangenberg, Loic Mager, Huriye Akdas-Kilig, Jean-Luc Fillaut, Bertrand Caro, Françoise Robin-Le Guen

Synthesis, Photophysics and Non-linear Optical Properties of Stilbenoid Pyrimidine-based Dyes bearing Methylenepyran Donor Groups

Sylvain Achelle,*[a] Jean-Pierre Malval,*[b] Stéphane Aloïse,[c] Alberto Barsella,[d] Arnaud Spangenberg,[b] Loic Mager,[d] Huriye Akdas-Kilig,[e] Jean-Luc Fillaut,[e] Bertrand Caro,[a] and Françoise Robin-le Guen[a]

[a] Dr. S. Achelle, Pr. B. Caro, Pr. F. Robin-le Guen

Institut des Sciences Chimiques de Rennes UMR CNRS 6226

IUT de Lannion

rue Edouard Branly, BP 30219

22302 Lannion Cedex, France

Fax: (+33) 2 96 46 93 54

E-mail: sylvain.achelle@univ-rennes1.fr

[b] Dr. J.-P. Malval, Dr. A. Spangenberg

Institut de Science des Matériaux de Mulhouse, UMR CNRS 7361

Université de Haute-Alsace

15 rue Jean Starcky,

68057 Mulhouse, France

E-mail: jean-pierre.malval@uha.fr

[c] Dr. S. Aloïse

Laboratoire de Spectrochimie Infrarouge et Raman, UMR CNRS 8516.

Université des Sciences et Technologies de Lille.

59655 Villeneuve d'Ascq Cedex. France

{d] Dr. A. Barsella, Dr Loic Mager

Département d'Optique ultra-rapide et Nanophotonique,

IPCMS-CNRS 23 Rue du Loess, BP 43,

67034 Strasbourg Cedex 2, France

[e] Dr. H. Akdas-Kilig, Dr. J.-L. Fillaut

Institut des Sciences Chimiques de Rennes UMR CNRS 6226,

Campus de Beaulieu, 263 av. du Général Leclerc,

35042 Rennes, France

Abstract

The nonlinear properties and the photophysical behavior of two π-conjugated chromophores incorporating an electron-deficient pyrimidine core (A) and γ-methylenepyrans as terminal donor (D) groups have been thoroughly investigated. Both dipolar and quadrupolar branching strategies are explored and rationalized on the basis of the Frenkel exciton model. Even though a cooperative effect is clearly observed when increasing the dimensionality, the NLO response of this series is moderate when considering the nature of the D/A couple and the size of the chromophores (as measured by the number of π electrons). This effect was assigned to a disruption of the electronic conjugation within the dyes scaffold whose geometry deviates from planarity due to a noticeable twisting of the pyranylidene end-groups. This latter structural parameter has also a strong influence on the excited-state dynamics which leads to a very efficient fluorescence quenching.

Introduction

In recent years, there has been a rapid progress in the development of nonlinear optical (NLO) materials due to their great impact and promising potentials in a wide range of applications such as multiphoton microscopy,[1] photodynamic therapy,[2] optical limiting,[3] multiphoton fabrication[4] or high density optical data storage.[5] A fundamental issue which constitutes the

cornerstone of all these applications concerns the elaboration of valuable design strategies to tune methodically the NLO response of the materials. Some key principles and structure-property relationships have been clearly identified especially for organic materials.[6] One of the simplest integrated systems consists in connecting together an electron–donor (D) and an electron–acceptor (A) group using a π-conjugated bridge as 'electron relay'. Within this prototypal dipolar configuration, several parameters account for the choice of the central π-conjugated fragment: i) the nature of linkers (double vs. triple bond)[7] ii) the size of the bridge as measured by the number of π electrons.[8] iii) the donor or acceptor character of the bridge iv) the inherent rigidity or flexibility of the bridge v) the aromatic character of the bridge. Several π-spacers have been successfully employed such as phenylene-vinylene,[9] phenylene-ethynylene,[7] fluorene,[10] dithienothiophene,[11] porphyrin.[12] A second fruitful strategy consists in increasing the dimensionality of the molecule with a recursive implementation of several D-π-A chromophores into a multibanched configuration[13] present in quadrupoles,[9b],[14] octupoles[13],[14c],[15] or dendrimers.[16] Due to a cooperative interaction among each arm, magnitude of the resulting NLO response is found to be much greater than the sum of the discrete NLO responses.

In line with this branching strategy, this paper presents the photophysical feature of two chromophores resulting from the molecular association of a new D/A couple linked by flexible phenylene-vinylene bridges (Scheme 1). The acceptor subunit is a substituted pyrimidine ring (1,3-diazine) which has been extensively used as building blocks for the synthesis of functionalized π-conjugated NLO materials.[17] The structural shape of the investigated pyrimidines gives rise to either one-dimensional or two-dimensional D-π-A or D-π-A-π-D type, respectively. The donor terminal group is a γ-methylenepyran system which is considered as a 'proaromatic' donor[18] since it gains aromaticity through charge transfer process. This effect obviously influences the degree of mixing between the quinoidal and

zwitterionic limiting resonance forms of ground state. As previously emphasized[19] the NLO properties are directly connected to the optimization of this latter degree of mixing. In the present contribution, we show that the twist angle within stilbenoid pyrimidine-based dyes bearing methylenpyran donor groups has a strong influence on the NLO properties but also drives the major relaxation process at excited state in this series.

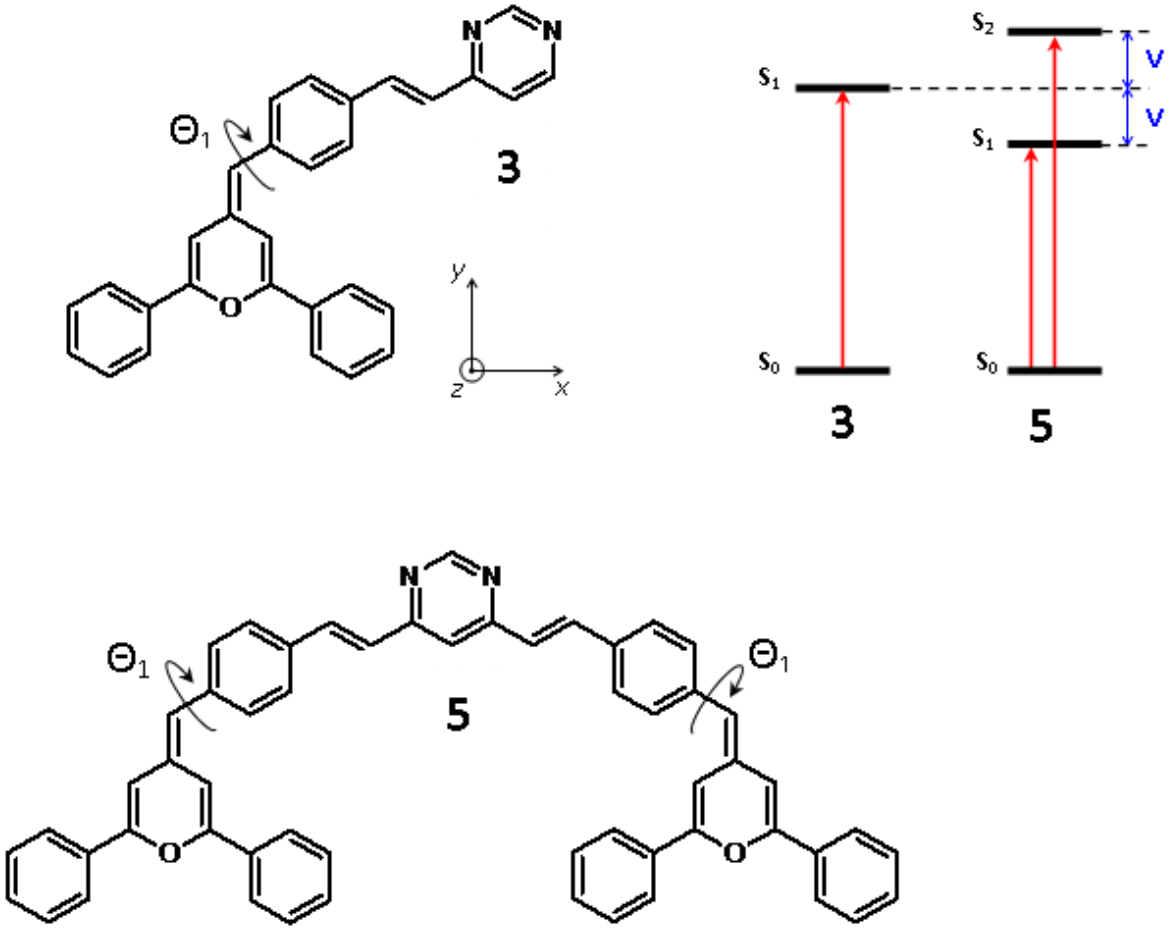

Scheme 1. Molecular structures of chromophores. Schematic representation of the effects of the interbranch coupling on the electronic levels on going from **3** to **5**.

Results and Discussion

Synthesis

The linear push-pull compound **3** has been obtained in two steps from readily available 4-methylpyrimidine (Scheme 2). The first step consists in a condensation reaction between 4-methylpyrimidine and 4-(diethoxymethyl)benzaldehyde in boiling aqueous 5M NaOH using Aliquat® 336 as a phase-transfer catalyst followed by deprotection of the acetal group in acidic media leading to compounds **1** according to the procedure initially described by Vanden Eynde.[20] The second step consists in a Wittig reaction between aldehyde **1** and phosphonium salt **2**[21] leading to compound **3**.[22] Quadrupolar derivative **5** has been obtained by the same synthetic procedure starting from 4,6-dimethylpyrimidine (Scheme 3). These materials are perfectly stable in the solid state and can be stored without the need for special precautions.

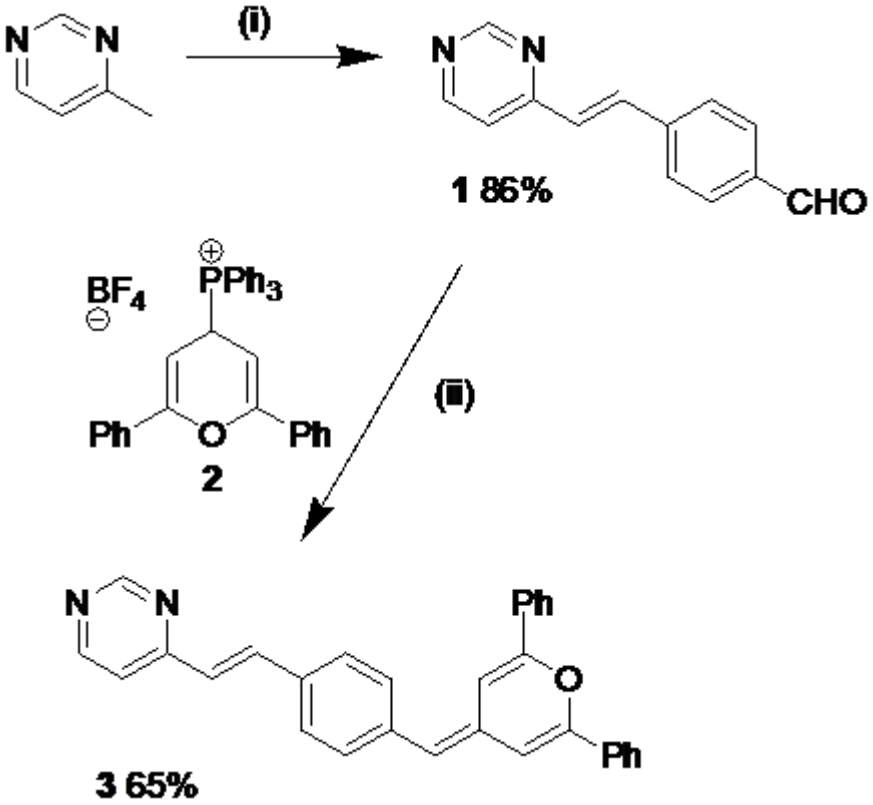

Scheme 2. Reaction scheme for the formation of **3**. (i) 4-(diethoxymethyl)benzaldehyde, Aliquat 336, 5M NaOH aq, 2h, Δ then HCl, acetone, 5 min room temp. (ii) *n*BuLi, THF, 2h, -78°C → RT.

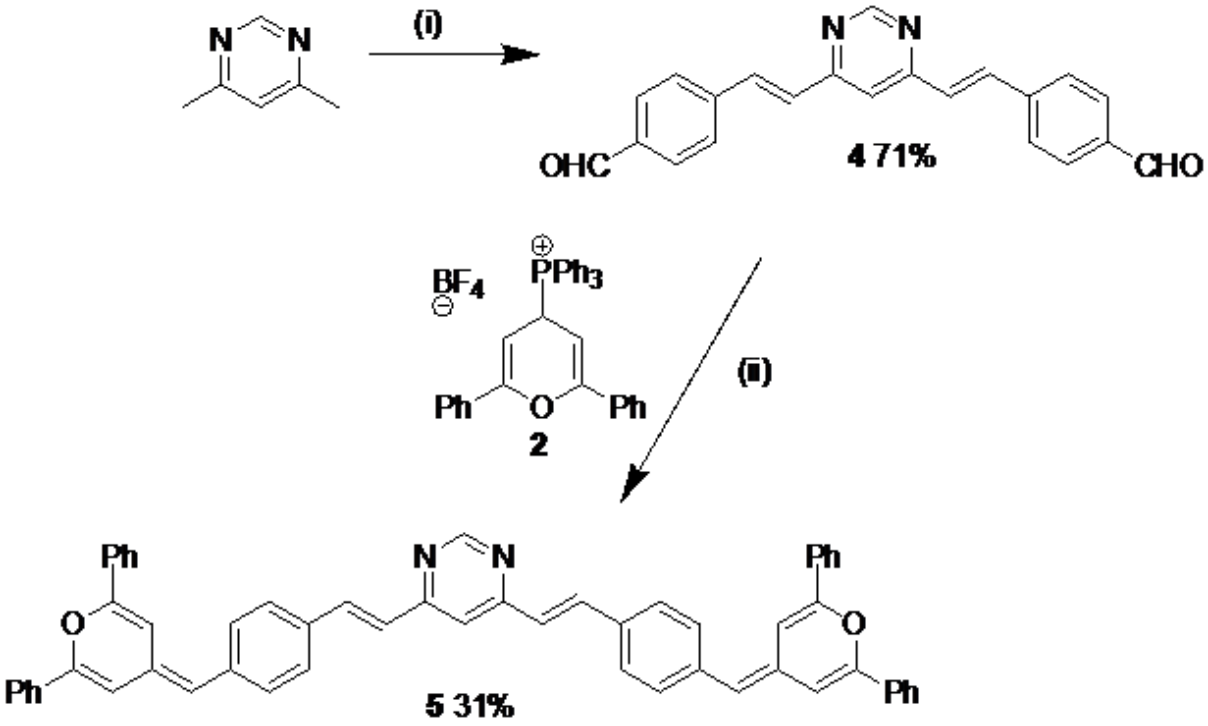

Scheme 3. Reaction scheme for the formation of **5**. (i) 4-(diethoxymethyl)benzaldehyde, Aliquat 336, 5M NaOH aq, 2h, Δ then HCl, acetone, 5 min room temp. (ii) *n*BuLi, THF, 2h, -78°C → RT.

Electronic and linear absorption properties of the ground state.

Figure 1 shows the absorption spectra of **3** and **5** in dichloromethane. Both dyes exhibit three absorption peaks at around 255, 290 and > 400 nm. It is noteworthy that a slight shoulder located at the blue edge of the longest wavelength absorption band is observed for compound **5**. The UV absorption band at 255 nm should be ascribed to the presence of the ^1L_a and ^1L_b electronic transitions centered on the 4-methylene-4H-pyran moiety.[23] Interestingly, this band is 2-fold intensive for the two-arm chromophore as compared to the dipolar one. Such a linear correlation first indicates that, for chromophore **5**, no intramolecular interaction at ground state occurs between the pyranylydene groups and that the electronic conjugation

between the 4-methylenepyran and the pyrimidine-based fragments remains comparable to that observed for **3** despite the increase of the dimensionality for the V-shaped structure. The fully optimized structures calculated at DFT level are presented in Figure 2. Both dyes show quite similar geometries. The 4-methylenepyran and the 4-styrylpyrimidine fragments adopt a quasi-planar conformation but are twisted between each other leading to a torsional angle (Θ_1 in Scheme 1) of about ~ 28°. Such a twisted geometry is independent of the substitution effects on the pyrimidine core. Moreover increasing the 2-dimensionality on going from a 4-(styryl) to a 4,6-bis(styryl)pyrimidine subunit hardly affects the planarity observed between the pyrimidine and its styryl substituents, resulting in hyperchromic and bathochromic effects. The longest wavelength absorption band which should encompass several π-π* electronic transitions partially localized on the substituted pyrimidine moiety shifts to low energy side of the spectrum and undergoes a 1.65-fold increase in intensity with ε_{max} of ca. 40 900 M^{-1} cm^{-1} and 67 400 M^{-1} cm^{-1} for compounds **3** and **5** respectively.

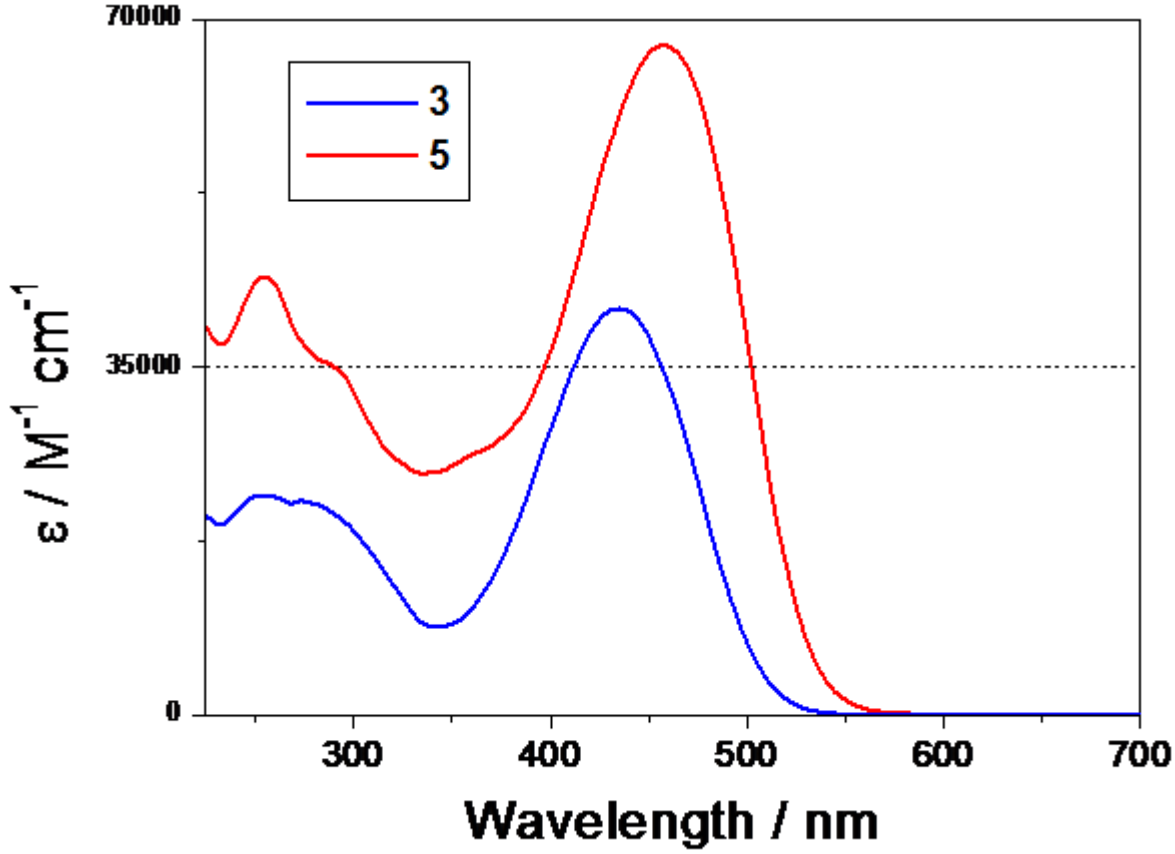

Figure 1. Absorption spectra of derivatives in dichloromethane.

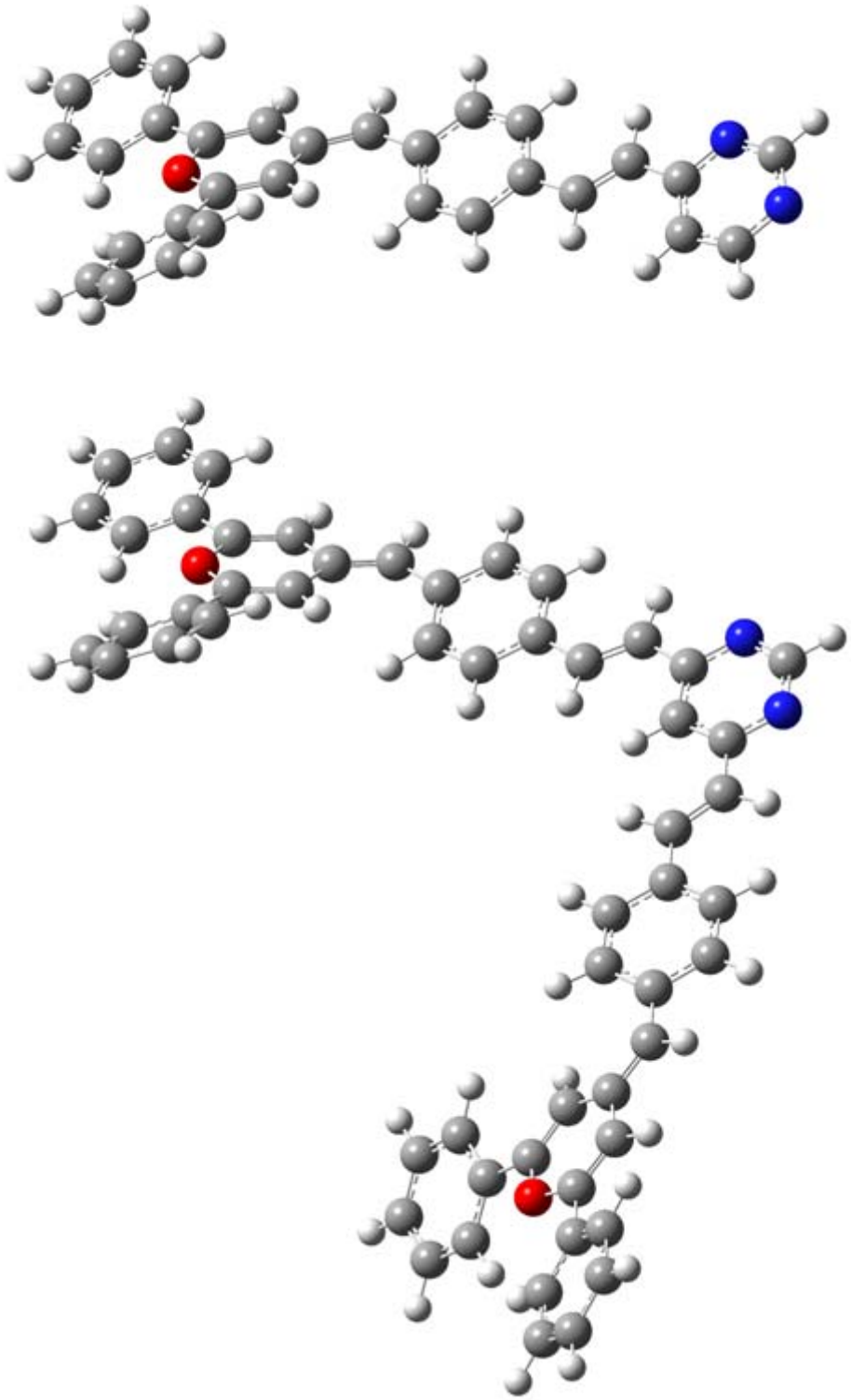

Figure 2. Optimized geometry of chromophores (PBE0/6-31G(d) level).

Figure 3 displays the cyclic voltamogramms of the derivatives in dichloromethane. Each compound exhibits an irreversible electrochemical oxidation wave with a peak at 0.73 V and 0.78 V vs. SCE for **3** and **5** respectively. These anodic potentials should be assigned to the oxidation of the methylenepyran group which probably leads to the formation of dimer by-products as previously observed for similar derivatives.[22],[24] Interestingly the oxidation potentials of both compounds are quite comparable. This effect should be connected to the equivalent degree of electronic conjugation between the pyran and styrylpyrimidine subunits within both chromophores which is consistent with the equivalent twisted geometries derived from DFT calculations. It was previously established that the oxidation potential of the methylenepyran group is strongly sensitive to the substituent on the exocyclic C=C bond. For instance, with a phenyl substituent, E_{ox} is about 0.73 V vs. SCE and strongly increases to 1.03 V vs. SCE with a 4-pyridyl group.[25] Therefore, the oxidation potentials obtained for **3** and **5** denotes the rather low communication between the two heterocycle parts of the molecules.

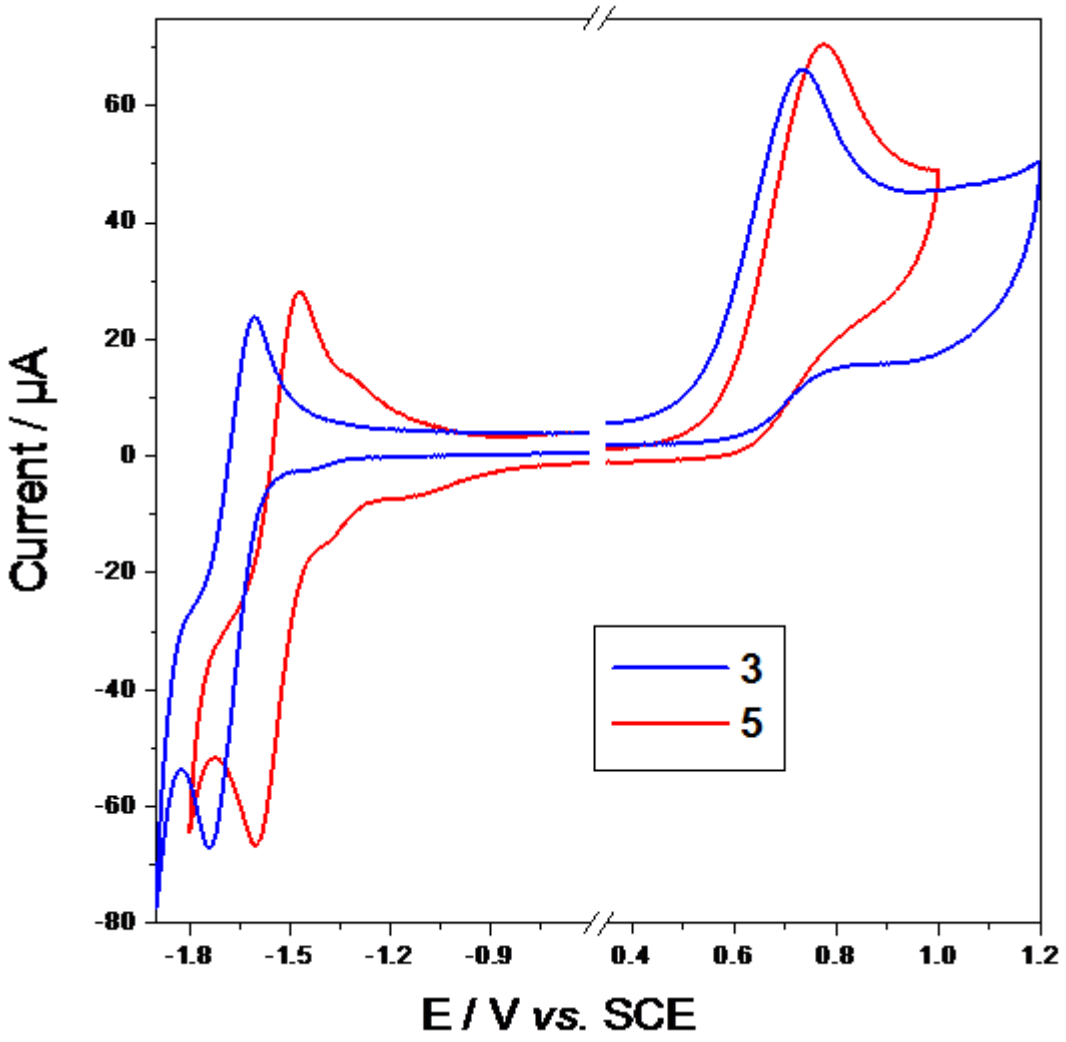

Figure 3. Cyclic voltamogramms of **3** and **5** in dichloromethane + $(nBu)_4NPF_6$ (0.1 M) on platinum electrode at 200 mV s^{-1} (concentrations within mM range).

The cathodic part of both voltamogramms shows a quasi reversible reduction wave with a half-wave potential of ca. -1.68 V vs. SCE for **3** and -1.53 V vs. SCE for **5**. This reduction wave corresponds to the formation of a radical anion located on the pyrimidine moiety. It is strongly shifted to the high potential region with respect to that of the pyrimidine (i.e. -2.56 V vs. SCE).[26] Such an electrochemical effect was previously observed for 4,6-dithienyl or 4,6-diarylpyrimidine derivatives[26],[27] and should be ascribed to an efficient stabilization of the

generated radical anion due to a charge delocalization along the styryl branches. The extending charge delocalization within the multibranched chromophore **5** stabilizes all the more the radical anion and leads to a further increase of the reduction potential (i.e. + 150 mV) with respect to that of **3**.

Figure 4 shows the steady-state excitation anisotropies of **3** and **5** along with their respective absorption and fluorescence spectra recorded in glassy matrix of 2-methyl tetrahydrofuran (2MTHF). The calculated absorption spectra using TD-DFT method are also displayed on top of each experimental spectrum. The electronic distributions of the frontier orbitals are shown in Figure 5. The calculated energies of the electronic $S_0 \rightarrow S_n$ transitions and the experimental values of the 0-0 transition energies (E_{00}) are reported in Table 1. The vertical $S_0 \rightarrow S_1$ transition energies agree well with the experimental E_{00} values, measured from the intercept of the normalized absorption and fluorescence spectra recorded at 77K in glassy matrix of 2MTHF. In the case of **3**, the constant anisotropy within the long wavelength absorption band (410-530 nm) is consistent with the presence of a single electronic transition. The calculations indicate that this $S_0 \rightarrow S_1$ transition is a pure HOMO-LUMO transition with a high oscillator strength ($f > 1$). This transition implies some delocalization of charge all along the chromophore with a pronounced localization on the donor group (methylenepyran) in the HOMO and on the pyrimidine acceptor in the LUMO. Below $\lambda_{exc} \approx 400$ nm, the anisotropy strongly decreases which suggests the presence of other electronic transitions with distinctive electronic symmetries.

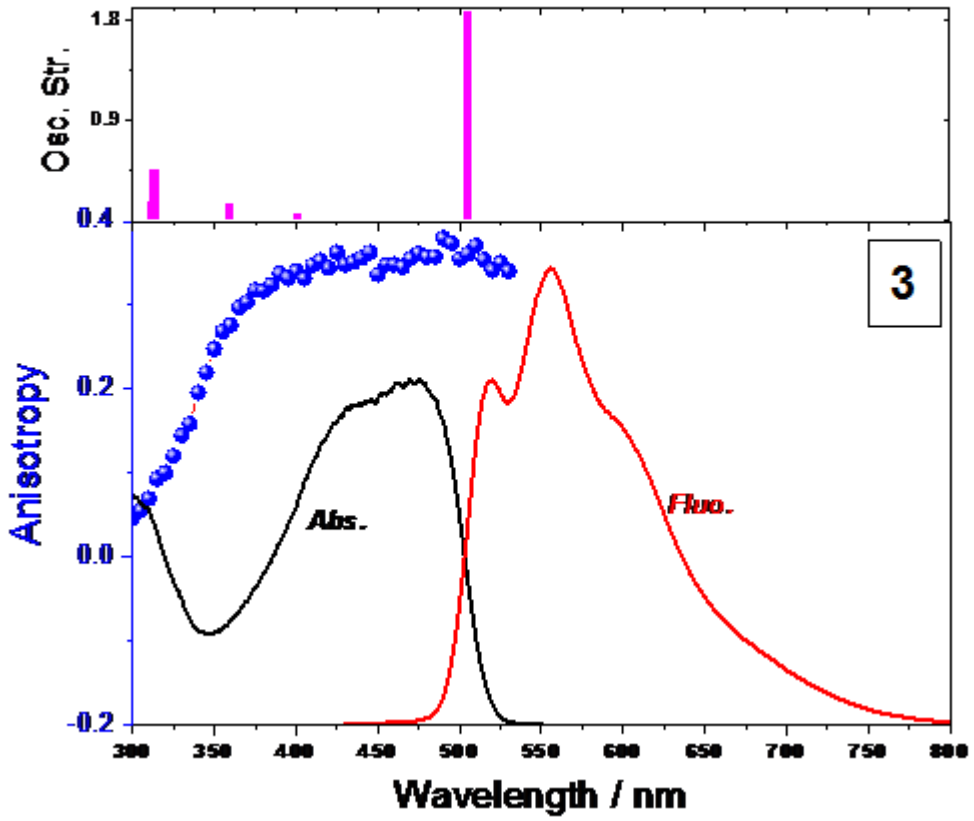
Osc. Str.
1.8
0.9
0.4
3
Anisotropy
0.2
0.0
-0.2
Abs.
Fluo.
300
350
400
450
500
550
600
650
700
750
800
Wavelength / nm

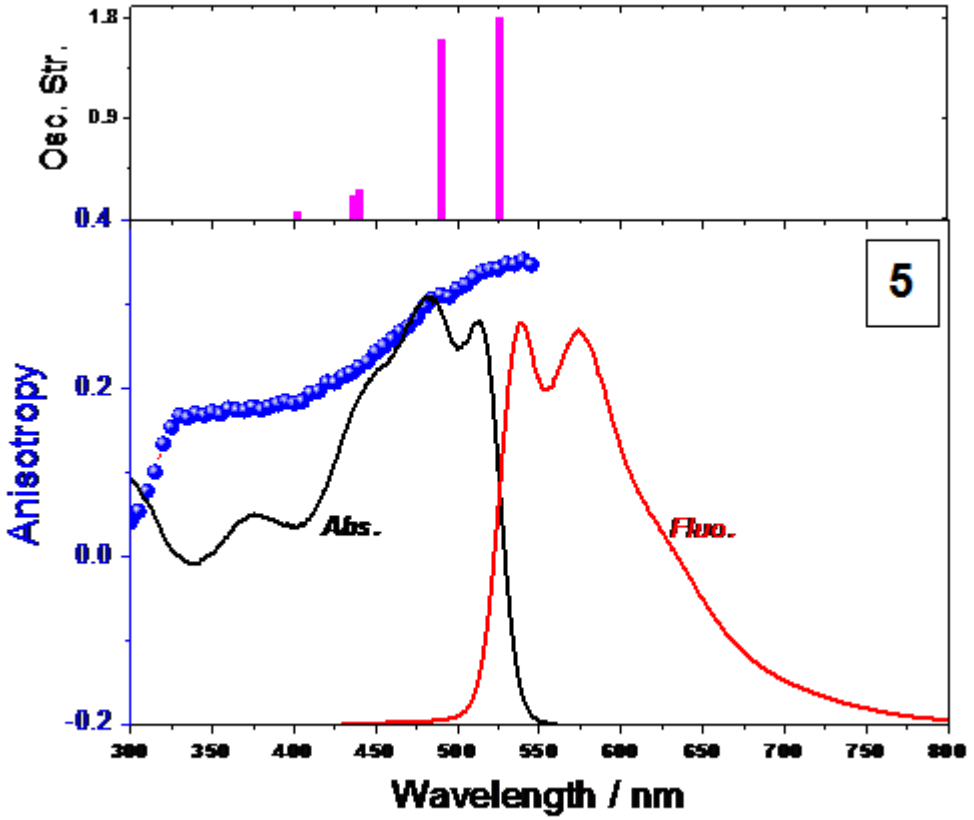
Osc. Str.
1.8
0.9
0.4
5
Anisotropy
0.2
0.0
-0.2
Abs.
Fluo.
300
350
400
450
500
550
600
650
700
750
800
Wavelength / nm

Figure 4. (Top) Positions of vertical energy transitions along with corresponding electronic oscillator strengths calculated from the TDDFT method. (Bottom) Normalized absorption and fluorescence spectra (full lines) of chromophores in glassy matrix of 2-MTHF (77K). Excitation anisotropy spectra (circles) in glassy matrix of 2-MTHF (77K).

The evolution of the excitation anisotropy spectrum of **5** is less straightforward. On going from 545 to 480 nm the anisotropy decreases sequentially from two narrow plateaus, then undergoes a strong drop below 475 nm and remains constant in the 400-330 nm range. These changes in the anisotropy spectrum are consistent with TD-DFT calculations which predict the occurrence of two energetically close and strongly allowed transitions which dominate the longest wavelength absorption band. The $S_0 \rightarrow S_1$ transition mainly corresponds to the HOMO-LUMO (73%) transition whereas the $S_0 \rightarrow S_2$ one implies a major contribution (70 %) from the $HOMO_{-1}$-LUMO (see Figure 5 for orbitals symmetry). Both transitions clearly correspond to conjugated π-π^* transitions and exhibit a charge transfer from the periphery (pyran fragments) to the core (pyrimidine ring) of the dye.

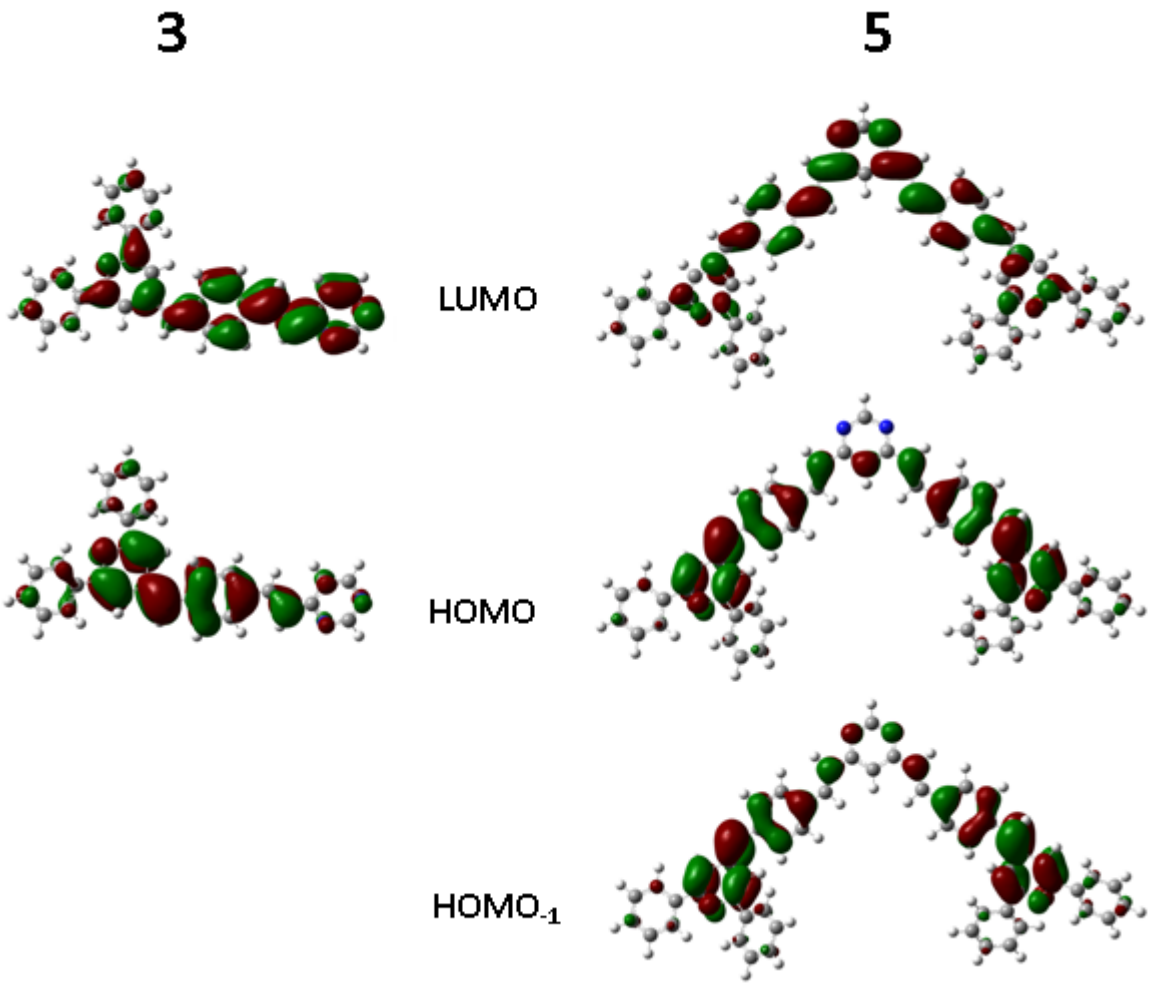

Figure 5. Representation of the molecular orbitals involved in the lowest energy electronic transitions of chromophores **3** and **5**.

The occurrence of these two transitions is well predicted within the framework of the Frenkel exciton model.[13],[28] For a two-branched V-shaped chromophore, it is assumed that interbranch electrostatic interactions lead to the splitting of the one-exciton transition relative to the molecular synthon.[29] This twofold degeneracy occurs symmetrically for a homo-dimeric chromophore (see inset of Scheme 1) and leads to a S_1-S_2 gap of 2V where V denotes the interbranch coupling. Such a symmetrical splitting is well reproduced here: calculations show that the midpoint energy between the S_1 (2.37 eV) and S_2 (2.53 eV) levels of chromophore **5** matches the S_1 energy of **3** (i.e. 2.46 eV). The interbranch coupling can be

estimated to ca. 0.09 eV. This value is moderate with respect to interbranch couplings calculated in the 0.15-0.20 eV range for symmetrical V-shaped structures bearing strong electron-withdrawing groups.[14c,d],[15a] This moderate coupling should indicate a weak dipole moment change upon dye excitation from ground to Franck-Condon states. In high energy region (i.e. λ_{exc} < 475 nm), two sets of two close lying transitions are predicted. The first set (namely $S_0 \rightarrow S_3$ and $S_0 \rightarrow S_4$) is positioned within the region that corresponds to the strong change of the anisotropy spectrum. This latter effect should be ascribed to an important change in the relative orientation of the transition dipole moments associated to each transition (see Table 1). Interestingly, the second set of $S_0 \rightarrow S_n$ transitions located around 400 nm are weakly allowed (f < 0.1) but exhibit similar electronic polarizations in line with the constant anisotropy observed in this spectral region.

Two photon absorption properties

The two-photon absorption spectra have been measured in the 740-980 nm range using the open aperture Z-scan technique.[30] Figure 6 shows the one- (1PA) and two-photon (2PA) absorption spectra of the compounds. The 2PA bands are plotted against half the excitation wavelength to have a direct comparison with the linear absorption spectra. According to our spectral resolution, it appears that the lowest energy 2PA band of **3** matches reasonably that of its 1PA one and shows a maximum 2PA cross-section (δ) of 86 ± 9 GM at 880 nm. Despite the strong electron-withdrawing character of the pyrimidine core and the good electron-donating ability of the pyran group whose oxidation potential is equivalent to that of a N,N' dimethylaniline (0.78 V vs. SCE),[31] the δ_{max} value obtained for **3** is relatively weak with respect to 2PA cross-sections of other linear 'push-pull' stilbenoid systems. For instance, the 4-dialkylamino-4'-nitrostilbene[32] or the 4-alkoxy-4'-nitrostibene[33] exhibit a δ_{max} of about 191 GM and 180 GM respectively. Cui *et al.*[34] reported that an electron deficient triazine core connected by a vinylene linker to dimethylaniline group leads to a δ_{max} of 340 GM. In

addition, if we normalize the 2PA cross-section by the effective number of π electrons (N_e) as proposed by Kuzyk *et al.*[8] the weak 2PA ability of **3** becomes even more sizeable since the ratio δ/N_e drops to 2.7 for **3** which is 5-times lower than the δ/N_e values for the other cited stilbenes.

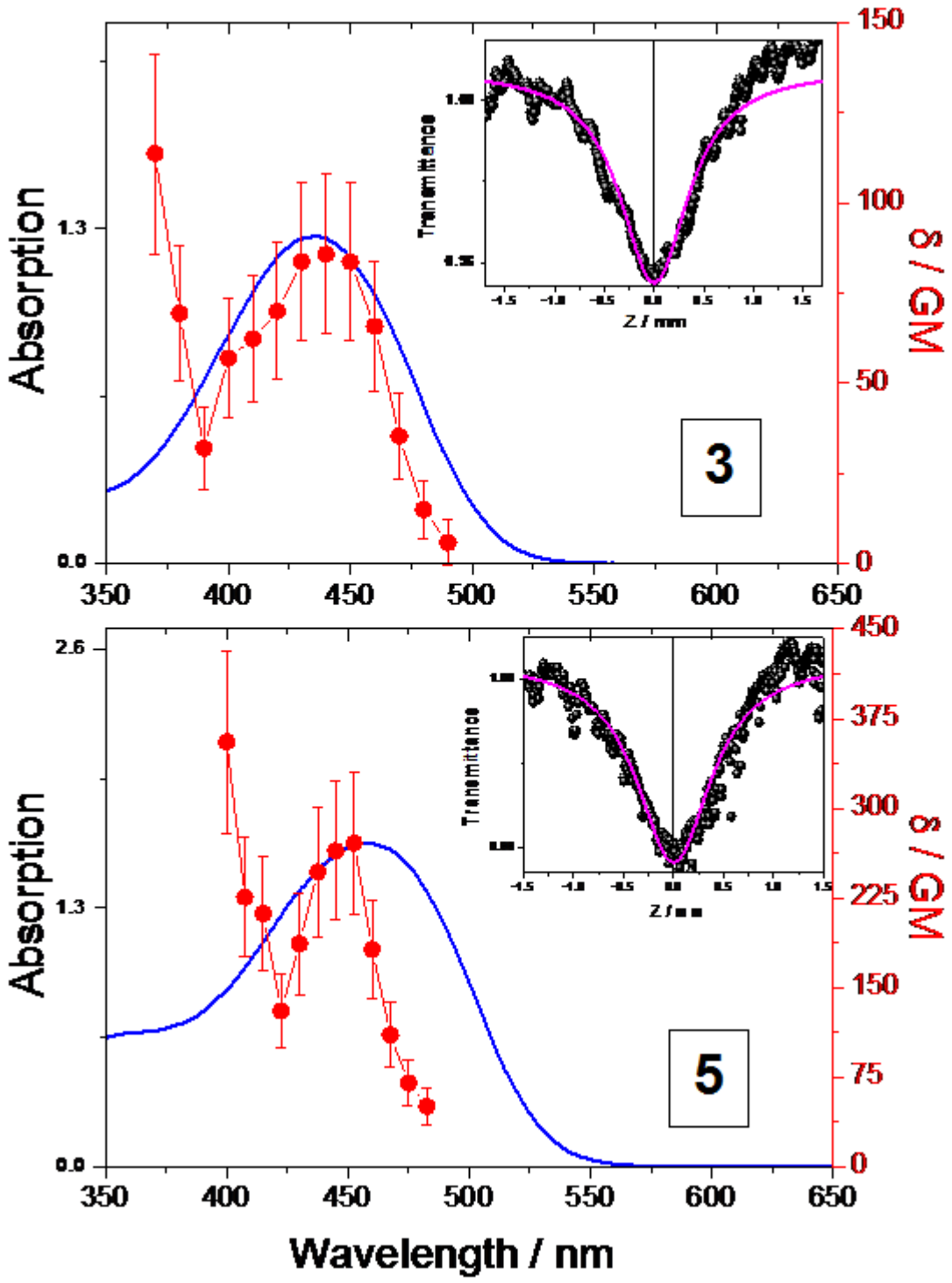

Figure 6. One- (full lines) and two- (data points) photon absorption spectra of dyes in dichloromethane. (The 2PA spectra are plotted against half the excitation wavelength).Inset: Typical Z-Scan graph and its best fitting curve (see text).

We assume that the flexible single bond which connects the stilbenyl moiety to the terminal donor group affects noticeably the non linear absorption properties of our derivatives. The flexible rotation between the donor and acceptor subunits (i.e. Θ_1 in Scheme 1) does not guarantee an optimum planar geometry that should maximize the π-orbital overlap. Such an influence of the twisted geometry on the 2PA cross-section was rationalized by Ahn *et al.*[12a] for a series of meso-linked porphyrin dimers which exhibit a gradual increase of the twist angle between the two porphyrins. On going from a near planar to perpendicular structure, the 2PA cross-section collapses by a factor 75. As shown in Figure 6, the 2PA maximum of the two-branched chromophore **5** is blue-shifted with respect to twice its linear absorption maximum. This should be ascribed to the nearly centrosymmetry of the D-π-A-π-D dye which leads theoretically to a two-photon forbidden $S_0 \rightarrow S_1$ transition. The longest wavelength 2PA band of **5** shows a maximum located around 900 nm with δ_{max} of 271 ± 28 GM which leads to a δ/N_e of about 4.7. Therefore, a cooperative enhancement of the 2PA efficiency is clearly evidenced on going from one-dimensional D-π-A system to a quadrupolar branching structure.

Second-order non-linear measurements.

Second-order non-linear properties have been studied in $CHCl_3$ solution using the electric-field-induced second-harmonic generation technique (EFISHG) which provides information about the scalar product μβ (2ω) of the vector component of the first hyperpolarisability tensor β and the dipole moment vector.[35] This product is derived according to eq. 1 and, considering that $\gamma_0(-2\omega,\omega,\omega,0)$, the third-order term, is negligible for the push-pull compounds

under study. This approximation is usually used for push-pull organic and organometallic molecules.

$$\gamma_{EFISH} = \mu\beta/5kT + \gamma_0(-2\omega,\omega,\omega,0) \quad (1)$$

Measurements are performed at 1907 nm, obtained from a Raman-shifted Nd:YAG$^+$ laser source, which allowed us to work far from the resonance peaks of the compounds we investigated (**3** and **5**). μβ values of 400 and 770 10^{-48} esu were obtained respectively for compound **3** and **5**. The μβ values of the two compounds are positive, indicating that excited state are more polarized than the ground state (μe > μg). In addition, this implies that the ground and excited states are polarized in the same direction. The positive values are in accordance with the emission solvatochromism observed for the compounds (see later). The μβ value obtained for compound **3** is higher than the value obtained for a 4-styrylpyrimidine substituted by a dimethylamino group (330 10^{-48} esu).[17b] It should be noted that, the D-π-A-π-D dye **5** is not completely symmetric has shown on DFT optimized geometry. This compound exhibit a higher μβ value than the dipolar compound **3**.

Excited-states properties.

Both chromophores are non fluorescent in apolar and low polar solvents (e.g. hexane or ethyl ether) at room temperature, and are weakly emissive when increasing solvent polarity (see Table 2). **5** is more emissive than **3**. In dichloromethane, the fluorescence quantum yield (Φ_f) is about 10^{-3} for **3** and 2.5 x 10^{-3} for **5**. In both cases, the structureless fluorescence band is very broad (Full width at half maximal FWHM ~ 4500 cm^{-1}) and is located in the 450-800 nm range (see Figure S1). **3** and **5** clearly exhibit a strong Stokes shift ($\Delta\upsilon_{ST}$) which increases with solvent polarity. The fluorescence spectrum undergoes a pronounced bathochromic

effect while only a small solvent-induced shift is observed for the absorption band, whith increasing the solvent polarity. This provides a clear evidence for a significant electronic and/or geometrical change between ground and emitting states.

The dipole moment change ($\Delta\mu_{ge}$) between ground and excited states can be estimated using the Lippert-Mataga equation[36] (eq. 2):

$$\Delta\nu_{ge} = \frac{2\Delta\mu_{ge}^2}{hca_0^3}\left(\frac{\varepsilon-1}{2\varepsilon+1}-\frac{n^2-1}{2n^2+1}\right)+Const \quad (2)$$

Within this dielectric continuum model, ε is the relative permittivity and n the refractive index of the solvent, h is the Planck constant and c is the speed of light. The Onsager radius a_0 defined as the solvent shell around the molecule was estimated to a value of ca. 5.5 Å for both molecules. This value corresponds to 40 % of the longest axis of the compound **3** as suggested by Lippert for non-spherical molecules.[36a] It should be emphasized that, for chromophore **5**, we assume that the relaxed S_1 state is not fully delocalized within the entire two-branched structure but is mainly localized on a single branch of the molecule. Such an assumption has been theoretically predicted for the relaxed S_1 state of multibranched chromophores with quadrupolar V-shaped geometries[14d] or octupolar trigonal symmetries.[37] Even though the solvatochromic measurements are performed over a limited range of the solvent polarity scale, the dipole moment change ($\Delta\mu_{ge}$) can be estimated to 15 ± 1 D and 19 ± 2 D for chromophores **3** and **5** respectively. Such values are of the same magnitude as those obtained for 'push-pull' trans-stilbenes such as 4-cyano-4'-dimethylaminostilbene[38] (~ 15 D) or 4-methoxy-4'-nitrostilbenes[33],[39] (~ 23 D) and therefore illustrate the significant CT character of the emitting states.

The very low fluorescence quantum yield measured for **3** and **5** is a clear indication of the occurrence of very efficient nonradiative deactivation processes at singlet excited state. We

assume that the main relaxation process responsible for the fluorescence quenching of **3** an **5** corresponds to a conformational change of the excited state.

Table 1. TDDFT and experimental electronic transitions of chromophores.

	3					**5**				
	Exp	*Theoretical*				*Exp*	*Theoretical*			
	E_{00} /eV	E_{th} /eV	f	Pol.[a]	Major natural transitions (fraction)	E_{00} /eV	E_{th} /eV	f	Pol.[a]	Major natural transitions (fraction)
$S_0 \rightarrow S_1$	2.47	2.46	1.872	<u>*x*,*y*</u> [b]	H-L	2.36	2.37	1.803	*y*	H-L (0.73), H_{-1}-L_{+1} (0.27)
$S_0 \rightarrow S_2$		3.09	0.064	*x*,<u>*y*</u> [b]	H_{-1}-L (0.54) , H_{-1}-L_{+1} (0.46)		2.53	1.598	*x*	H-L_{+1} (0.30), H_{-1}-L (0.70)
$S_0 \rightarrow S_3$		3.45	0.144	*x*,<u>*y*</u> [b]	H_{-1}-L_{+1}(0.46) , H-L_{+2} (0.54)		2.82	0.258	*x*	H_{-1}-L (0.31), H-L_{+1} (0.69)
$S_0 \rightarrow S_4$		3.96	0.455	*x*	H_{-2}-L (0.20) , H_{-1}-L (0.80)		2.84	0.211	*y*	H-L (0.27), H_{-1}-L_{+1} (0.73)
$S_0 \rightarrow S_5$		3.99	0.160	*y*	H_{-2}-L (0.69) , H_{-1}-L (0.18)[c]		3.08	0.067	<u>*x*</u>,*z*	H_{-1}-L_{+3} (0.27), H-L_{+3} (0.27)[c]
$S_0 \rightarrow S_6$		4.01	0.002	*z*	H_{-3}-L (0.64) , H_{-3}-L_{+1} (0.19)[c]		3.09	0.051	<u>*x*</u>,*z*	H-L_{+4} (0.18), H_{-1}-L_{+4} (0.19)[c]

[a] xyz axis are displayed in Scheme 1, [b] The main component is underlined, [c] The two principal natural transitions are displayed

Table 2. Spectroscopic data of the ground and excited states of compounds in various solvents.

	3					**5**				
Solvent	λ_a / nm	λ_f / nm	FWHM[a] / cm^{-1}	Φ_f x 10^2	Stokes Shift / cm^{-1}	λ_a / nm	λ_f / nm	FWHM[a] / cm^{-1}	Φ_f x 10^2	Stokes Shift / cm^{-1}
ETA	425	546	4690	0.04	5214	446	568	4145	0.12	4816
2MTHF	428	557	4840	0.04	5411	450	576	4334	0.13	4861
THF	431	556	4982	0.06	5216	452	577	4190	0.17	4793
DCM	436	566	4675	0.10	5268	458	609	4095	0.22	5414
ACT	427	581	4260	0.09	6207	447	630	4040	0.19	6498
DMF	434	592	4505	0.19	6150	456	652	4020	0.28	6592

[a] Full width at half maximum for fluorescence bands.

Trans-to-*cis* photoisomerization should be first excluded as a major nonradiative channel. Indeed, the measured quantum yield for this photoreaction ($\Phi_{t\rightarrow c}$) has a very low value (below 10^{-3}) both in hexane and DMF (N_2-degassed solutions). Such a weakly efficient photoisomerization is presumably due to a large activation barrier between the S_1 state and the double-bond-twisted excited species ^1P.[40] This so-called 'phantom' ^1P state acts as a photochemical funnel (possibly through conical intersection) toward the ground state surface from which an equally probable isomerization to *cis* and *trans* occurs.[41] We can also exclude

that a parallel photoisomerization reaction may occur via intersystem crossing (ISC).[42] In this case, the planar triplet state would undergo a barrierless C=C torsion to the ^{3}P state. However, one would expect that $\Phi_{t\rightarrow c}$ should be at least equal to half the value of Φ_{ISC} even though we ssume that the triplet state mechanism constitutes the major photoisomerization pathway. Due to the very low quantum yield measured for the photoisomerization (< 10^{-3}), intersystem crossing should be considered as a negligible process with respect to the other deactivation pathways at singlet excited state.

This assumption is also in line with the very weak phosphorescence measured for **3** and **5** in glassy matrix of 2-methyl tetrahydrofuran (2MTHF) (see Figure S2). The phosphorescence spectrum, located in the 600-750 nm region is strongly overlapped with the fluorescence band. This suggests a relatively small energy difference between S_1 and T_1 levels. As a consequence, a thermally activated delayed fluorescence emission is observed even at 77 K. Moreover the delayed fluorescence lifetime is quite similar to that obtained for phosphorescence emission with values of about 15 μs. Note that the very short lifetime measured for the phosphorescence of T_1 state is a clear indication of its nπ* character. Hence, it appears that additional nonradiative processes at S_1 state other than *trans*-to-*cis* photoisomerization and intersystem crossing should be taken into account to explain the very weak fluorescence of the chromophores at room temperature.

Finally, we observed that high-viscosity solvents freeze down the molecular relaxation precesses in **3** and **5**. Figure 7 displays the temperature dependence of steady-state fluorescence spectra of **3** and **5** in 2MTHF. First, it should be noted that the fluorescence quantum yields strongly increase upon cooling the solutions. From 293 K to 80 K Φ_f is multiplied by a factor 430 and 105 for **3** and **5** respectively. Two distinctive steps are clearly observed and both dyes behave similarly in a qualitative sense. Decreasing temperature from 293 K to 140 K results in a fluorescence enhancement of about ~ 8 and a gradual band

redshift with a thermochromic slope of ~ 11 $cm^{-1}K^{-1}$ for **3** and ~ 14 $cm^{-1}K^{-1}$ for **5**. Upon further cooling, the bathochromic effects level off and below 130 K the fluorescence bands reversely shift to the high energy region with a sizeable increase in intensity.

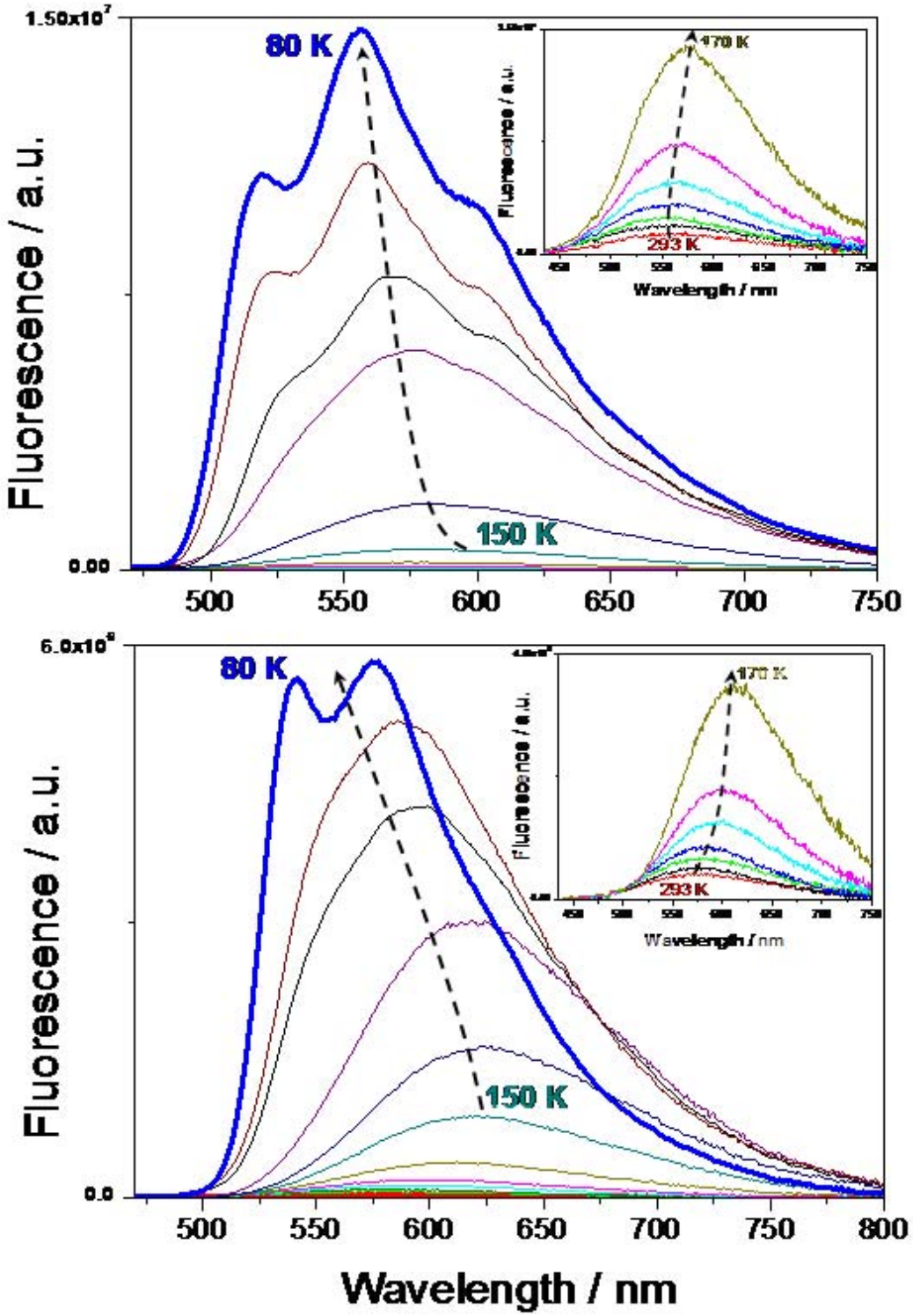

Figure 7. Fluorescence spectra of **3** and **5** in 2MTHF over the temperature range of 80-293 K.

It is well established that dielectric constant and viscosity are two main physical properties of the surrounding medium which affect the fluorescence properties of chromophores.[43] Concerning 2MTHF, the relative influence of these two parameters evolves sequentially depending on the temperature range.[44] In the high temperature region (i.e. above glass-transition temperature, Tg ~ 130 K), the thermochromic shift should be mainly ascribed to an increase of the effective solvent polarity due to a continuous growth of the dielectric constant from 7 at 293 K to a maximum value of 18 at 140 K.[45]. During the glass-transition step, the dielectric constant drops abruptly to 2.6 and remains quite constant from 110 K to 77 K. Meanwhile, the viscosity increases exponentially from 10^2 Pa.s to 3.5 x 10^{19} Pa.s. In this low temperature region, all conformational changes are severely restricted. This change of the solvent viscosity is clearly responsible for the dramatic fluorescence enhancement for **3** and **5** associated with a band hypsochromy. As a consequence, we propose that the main relaxation process responsible for the fluorescence quenching of **3** and **5** corresponds to a conformational change from a nearly planar locally excited (^{1}LE) state to a twisted geometry, presumably a twisted intramolecular charge transfer (^{1}TICT) state.[46] This D-A decoupled geometry is expected to exhibit a forbidden optical transition which leads to a non-emissive (or weakly emissive) excited state (see Scheme 4).

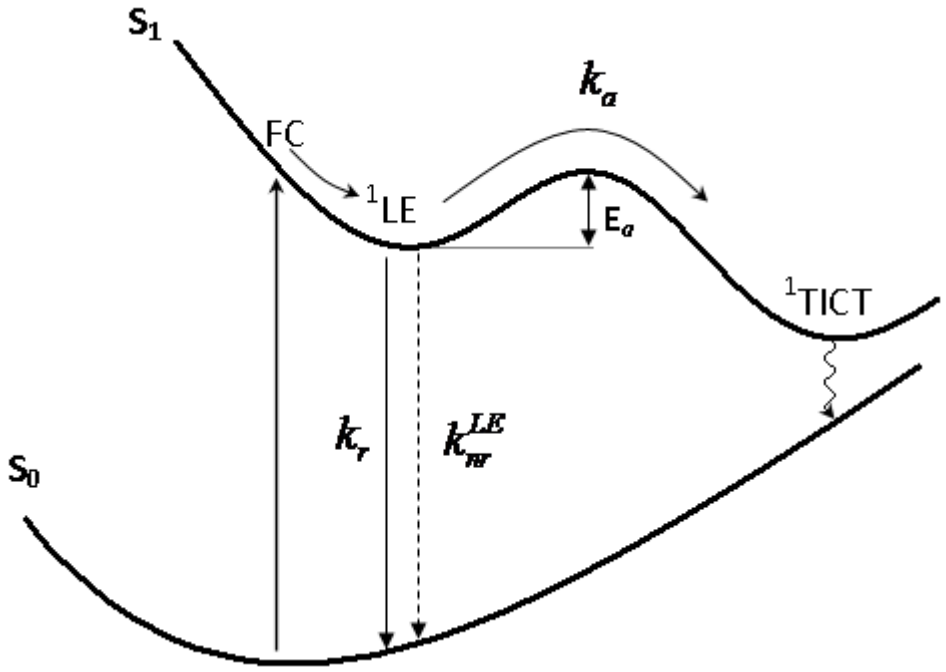

Scheme 4. Schematic representation of the adiabatic TICT reaction pathway.

In reference to donor-acceptor-substituted stilbenes, two scenarios can be investigated. They all rely on the molecular structure of the stilbene, the nature of the D/A couples and the determination of the single bond involved in the torsional motion. Interestingly both twisting mechanisms strongly compete with the formation of ^{1}P state which is consistent with the very low *trans*-to-*cis* quantum yields observed for **3** and **5**. A first mechanism was proposed by Rettig, Lapouyade *et al.* which is based n ring-bridged model stilbene derivatives.[38bc],[47] In this mechanism, the formation of the ^{1}TICT state results in a rotation about a single bond adjacent to the central ethylene one. This hypothesis was proposed, for of *trans*-4-(N,N-dimethylamino)stilbenes or *trans*-4-(alkoxy)stilbenes with strong terminal acceptor groups (e.g. –CN, $–NO_2$) in 4' position. Such a precursor-successor mechanism affects the central part of the chromophore. In our case, this relaxation mode would induce a very large amplitude motion when considering the crowded V-shaped structure of **5**. Therefore, one would expect a significant activation barrier (E_a) between ^{1}LE and ^{1}TICT states (see Scheme

4). Interestingly, these latter activation barriers can be determined for **3** and **5**. Indeed, the nonradiative rate constant (k_{nr}) can be derived from the following relationship:

$$\frac{k_{nr}}{k_r} = \frac{k_{IC} + k_{ISC} + k_a}{k_r} = \frac{1-\Phi_f}{\Phi_f} \quad \textbf{(3)}$$

In this equation, the radiative rate constant of the emitting state (k_r) is considered not to correlate with temperature and the internal conversion (IC) is normally an unactivated process.[48] If we assume that intersystem crossing can be neglected as compared to ^{1}LE→^{1}TICT process (k_a) and internal conversion then one can derive that $k_{nr} \approx k_{IC} + k_a$. The Arrhenius plots of ln(k_{nr}/k_r) vs. 1/T are presented in Figure 8 and correlations are sufficiently linear to derive activation barriers in the 1.7-1.8 kcal/mol range. These values nicely coincide to the solvent viscosity barrier (E_η ~1.82 kcal/mol for 2MTHF)[49] which indicates that the ^{1}LE→^{1}TICT reaction does not proceed over a significant activation barrier and does not require a large-amplitude conformational change from the ^{1}LE state. Therefore this first mechanism is not reasonably transposable to our chromophores.

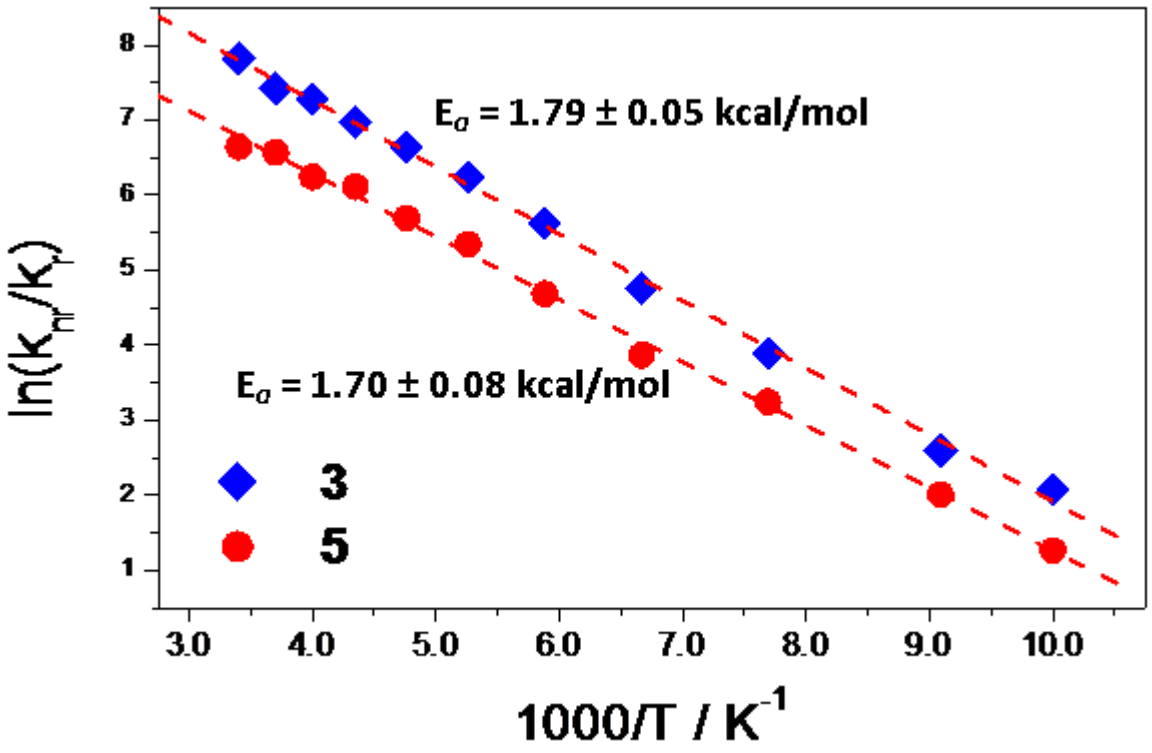

Figure 8. Arrhenius plot for the nonradiative-to-radiative rate constants ratio.

A second relaxation mechanism has been evidenced and extensively studied by Yang *et al.*[48a],[50] This model was proposed for some aryl-substituted stilbenes such as N-aryl-substituted *trans*-4-aminostilbenes. Note that the molecular structure of these derivatives is quite similar to that of our compounds. The conformation change at excited state results in a rotation about the single bond which connects the stilbenyl structure with the external aromatic subunit. This mechanism is more in line with the barrierless nature of the reaction since it only implies the relative motion of a peripherical part of the molecule with the rotation of a methylenepyran group from a twist angle of ~ 28° (see DFT calculation) to 90° with respect to the 4-styrylpyrimidine fragment (see Scheme 1).

Conclusion

A linear and a V-shaped pyrimidine-based chromophore bearing γ-methylenepyrans as terminal donor groups have been synthesized. According to a large set of experimental data supported by DFT theoretical calculations, the photophysical properties of these new NLO organic materials have been methodically untangled. The branching effect is well described within the Frenkel exciton model and leads to a moderate interbranch coupling. The ground state structure of both derivatives shows a significant twisting of the pyranilydene groups with respect to the planar electron-deficient pyrimidine core. Such a deviation from planarity of the chromophores does not allow an optimal electronic conjugation all along the molecular scaffold. As a consequence, the NLO response is modest as compared to that of other π-conjugated derivatives with similar size and architecture. In the same manner, the rotation of the donor end-group has a decisive influence on the excited-states dynamics which leads to a detrimental fluorescence quenching effect. Therefore we demonstrate here that the flexibility of a simple structural parameter both affects the NLO properties as well as the dyes

emissivity. Preventing this specific rotation would presumably lead to a synergetical effect. A ring-bridged strategy is currently underway.

Experimental Section

Materials and general methods. In air and moisture-sensitive reactions, all glassware was flame-dried and cooled under nitrogen. All other commercially available reactants are used without further purification. The solvents used for absorption and emission analysis are as follows: Ethyl acetate (ETA), 2-Methyl tetrahydrofuran (2MTHF), Tetrahydrofuran (THF), Dichloromethane (CH_2Cl_2), Acetone (ACT), Dimethylformamide (DMF). All the solvents employed were Aldrich, Fluka or Merck spectroscopic grade. Compounds **1** and **4** were prepared as previously described.[21b] NMR spectra were acquired at room temperature on a Bruker DRX500 spectrometer at the "Service Commun de Recherche de Résonance Magnétique Nucléaire et de Résonance Paramagnétique Electronique de l'Université de Bretagne Occidentale". Chemical shifts are given in parts per million relative to TMS (1H, 0.0 ppm) and $CDCl_3$ (13C, 77.0 ppm). Acidic impurities in $CDCl_3$ were removed by treatment with anhydrous K_2CO_3. High resolution mass analyses were performed at the "Centre Régional de Mesures Physiques de l'Ouest" (CRMPO, University of Rennes1) using a Bruker MicroTOF-Q II apparatus.

General procedure for Wittig reaction : Small excess of *n*-butyllithium (1.1 equiv.; 2.5 M in hexanes) was added dropwise at -78 °C, under a nitrogen atmosphere, to a degassed solution of 2,6- **Materials and general methods**. In air and moisture-sensitive reactions, all glassware was flame-dried and cooled under nitrogen. All other commercially available reactants are used without further purification. The solvents used for absorption and emission analysis are as follows: Ethyl acetate (ETA), 2-Methyl tetrahydrofuran (2MTHF), Tetrahydrofuran (THF), Dichloromethane (CH_2Cl_2), Acetone (ACT), Dimethylformamide (DMF). All the solvents employed were Aldrich, Fluka or Merck spectroscopic grade.

Compounds **1** and **4** were prepared as previously described.[21b] NMR spectra were acquired at room temperature on a Bruker DRX500 spectrometer at the "Service Commun de Recherche de Résonance Magnétique Nucléaire et de Résonance Paramagnétique Electronique de l'Université de Bretagne Occidentale". Chemical shifts are given in parts per million relative to TMS (1H, 0.0 ppm) and $CDCl_3$ (13C, 77.0 ppm). Acidic impurities in $CDCl_3$ were removed by treatment with anhydrous K_2CO_3. High resolution mass analyses were performed at the "Centre Régional de Mesures Physiques de l'Ouest" (CRMPO, University of Rennes1) using a Bruker MicroTOF-Q II apparatus.

General procedure for Wittig reaction : Small excess of *n*-butyllithium (1.1 equiv.; 2.5 M in hexanes) was added dropwise at -78 °C, under a nitrogen atmosphere, to a degassed solution of 2,6-diphenyl-4H-pyran-4-yl triphenylphosphonium tetrafluoroborate salt **2**[21] (1 equiv.) in dry THF. After 15 min, the carboxaldehyde (0.9 equiv. and 0.45 in case of compounds **4**) was added. The solution was stirred at -78°C for 30 min, and allowed to warm to room temperature for 2h. THF was evaporated and the residue dissolved in a mixture of CH_2Cl_2/water 1:1 (100 mL) and the organic layer separated. The aqueous layer was extracted with CH_2Cl_2 (2 x 50 mL). The combined organic extracts were dried with $MgSO_4$ and the solvents evaporated.

(E)4-{2-[4-(2,6-Diphenyl-pyran-4-ylidenemethyl)-phenyl]-vinyl}-pyrimidine (3) : Red solid; obtained according to general procedure and purified by column chromatography (SiO_2, CH_2Cl_2/ETA, 1:1) followed by crystallization from $CHCl_3$/n-heptane; yield 65% (277 mg); mp : 227-228 °C (dec); ^{1}H NMR (500 MHz, $CDCl_3$) δ 5.94 (s, 1H), 6.44 (s, 1H), 7.04 (s, 1H), 7.05 (d, 1H, *J* = 16 Hz), 7.31 (d, 1H, *J* = 5Hz), 7.46-7.42 (m, 8H), 7.59 (d, 2H, *J* = 8Hz), 7.78-7.76 (m, 4H), 7.89 (d, 1H, *J* = 16 Hz), 7.66 (d, 1H, *J* = 5 Hz), 9.16 (s, 1H); ^{13}C NMR and JMOD (125 MHz, $CDCl_3$) δ 162.5 (C), 158.9 (CH), 157.3 (CH), 153.3 (C), 151.3 (C), 140.3

(C), 137.3 (CH), 133.4 (C), 133.2 (C), 132.6 (C), 130.5 (C), 129.5 (CH), 129.2 (CH), 128.8 (CH), 128.70 (CH), 128.70 (CH), 128.1 (CH), 125.0 (CH), 124.6 (CH), 124.3 (CH), 118.6 (CH), 113.7 (CH), 108.7 (CH), 102.2 (CH). HRMS (ESI/ASAP) m/z calculated for $C_{30}H_{23}N_2O$ $[M+H]^+$ 427.1810, found 427.1804.

4,6-Bis-{2-[4-(2,6-diphenyl-pyran-4-ylidenemethyl)-phenyl]-vinyl}-pyrimidine (5) : Red solid; obtained according to general procedure and purified by column chromatography (SiO_2, CH_2Cl_2/ETA, 7:3) followed by crystallization from $CHCl_3$/n-heptane; yield 31% (240 mg); mp : 243-244 °C (dec.); ^{1}H NMR (500 MHz, $CDCl_3$) δ 5.95 (s, 2H), 6.45 (s, 2H), 7.06 (s, 2H), 7.08 (d, 2H, *J* = 16 Hz), 7.28 (s, 1H), 7.48-7.40 (m, 16H), 7.61 (d, 4H, *J* = 8Hz), 7.79-7.77 (m, 8H), 7.92 (d, 2H, *J* = 16 Hz), 9.10 (s, 1H); ^{13}C NMR and JMOD (125 MHz, $CDCl_3$) δ 162.9 (C), 158.7 (CH), 153.2 (C), 151.2 (C), 140.1 (C), 136.8 (CH), 133.4 (C), 133.2 (C), 132.8 (C), 130.5 (C), 129.5 (CH), 129.2 (CH), 128.71 (CH), 128.69 (CH), 128.1 (CH), 128.0 (CH), 125.0 (CH), 124.7 (CH), 124.6 (CH), 116.4 (CH), 113.8 (CH), 108.8 (CH), 102.2 (CH). HRMS (ESI) m/z calculated for $C_{56}H_{41}N_2O_2$ $[M+H]^+$ 773.3168, found 773.3163.

Steady-state absorption and fluorescence spectra. The absorption measurements were carried out with a Perkin Elmer Lambda 2 spectrometer. Steady-state fluorescence and phosphorescence spectra were collected from a FluoroMax-4 spectrofluorometer. Emission spectra are spectrally corrected, and fluorescence quantum yields include the correction due to solvent refractive index and were determined relative to quinine bisulfate in 0.05 molar sulfuric acid (Φ_{ref} = 0.52)[51] Due to the very weak emissive chromophores ($\Phi_f < 10^{-3}$), the fluorescence quantum yields were obtained from 5 independent measurements and the uncertainties were determined to ± 20 %. Phosphorescence and steady-state anisotropy measurements were performed in 2-methyl tetrahydrofuran at 77 K. The samples are placed in a 5-mm diameter quartz tube inside a Dewar filled with liquid nitrogen.

Time-gated luminescence. The phosphorescence lifetimes were measured using a FluoroMax-4 spectrofluorometer which is also equipped with a Xe-pulsed lamp operating at up to 25 Hz. The phosphorescence decays are obtained according to a time-gated method. The emission is recorded using a control module that includes a gate-and-delay generator which allows the integration of the signal during a specific period after a flash (delay) and for a pre-determined time window. The total signal is accumulated for a large number of exciting pulses.

Fluorescence anisotropy. For the steady-state anisotropy measurements, two Glan-Thompson polarizers are placed in the excitation and emission beams. The anisotropy r is determined as follows:

$$r = \frac{I_{VV} - gI_{VH}}{I_{VV} + 2.g.I_{VH}} \qquad g = \frac{I_{HV}}{I_{HH}}$$

Where I is the fluorescence intensity. The subscripts denote the orientation (horizontal H or vertical V) of the excitation and emission polarizers, respectively. g is an instrumental correction factor. The proper calibration of the set-up was checked using a recent standard method with rhodamine 101 in glycerol.[52]

Low-temperature measurements. Low-temperature emission measurements were performed in 2MTHF using a Oxford Cryogenics OptistatDN cryostat fitted with a Oxford Instruments ITC503S temperature controller. The temperature dependency of the refractive index and the density of the solvent were taken into account for the measurement of Φ_f.[53]

Cyclic voltammetry. The cyclic voltammetry experiments[54] (using a computer-controlled Radiometer Voltalab 6 potentiostat with a three-electrode single compartment cell; the working electrode was a platinum disk; a saturated calomel electrode (SCE) used as a reference was placed in a separate compartment with a salt bridge containing the supporting

electrolyte) were performed at 300 K, in N_2-degassed dichloromethane with a constant concentration (0.1 M) of n-Bu_4BF_4. Ferrocene (Fc) was used as an internal reference (considering $E_{Fc/Fc+}$ = 0.53 V in CH_2Cl_2 vs. aqueous SCE).[55]

Actinometry. Quantum yields for *trans* → *cis* photoisomerization were measured under irradiation at 436 nm using a 100 W Mercury-Xenon Lamp (Hamamatsu, L2422-02) equipped with a band pass filter (THORLAB, FB430-10). All irradiated solutions were previously N_2-degassed. The progress of the photoreaction was monitored via UV−vis absorption spectra. The absorbance at excitation wavelength was greater than 2 to assume a total absorption of the incident photons. The incident light intensity was measured by ferrioxalate actinometry.[56]

Open-aperture Z-scan method. The two-photon absorption spectra were measured using open-aperture Z-scan method[30] with a femtosecond mode-locked Ti: Sapphire laser (Coherent, Chameleon Ultra II : pulse duration: 140 ± 20 fs; repetition rate: 80 MHz; wavelength range: 680-1080 nm). After passing through a beam expander (x 4), the laser beam is focused using an f = 15 cm lens and passed through a quartz cell (1 mm optical path length). The position of the sample cell is varied along the laser-beam direction (z-axis) using a Z-step motorized stage controlled by a computer. At constant incident excitation, the local power density within the sample is changed and the corresponding transmitted laser beam, T(z), recorded with a silicon photodetector (Ophir PD300) is monitored in connection with the z-position of the cell. The on-axis peak intensity of the incident pulses at the focal point, I_0, ranged from 30 to 90 GW cm^{-2}. If we assume that the linear absorption of the sample is negligible at working wavelength and that the laser exhibits a Gaussian beam profile in space and time, the nonlinear absorption coefficient β can be calculated from the curve fitting to the experimental transmittance with the following equation:

$$T(z) = 1 - \frac{\beta I I_0}{2\sqrt{2}(1+(\frac{z}{z_0})^2)}$$

Where z_0 is the coordinate along the propagation direction of the focal point of the beam, l the optical path length. The 2PA cross-section, δ, (in units of 1 GM : 10^{-50} cm^4 s $photon^{-1}$ $molecule^{-1}$) is then determined by using the relationship:

$$\beta = \frac{\delta N_A d}{h\nu} 10^{-3}$$

Where h is the Planck constant, υ the frequency of the incident laser beam, N_A the Avogadro constant and d is the concentration of the chromophore (mol. L^{-1}). The rhodamine 6G in methanol[57] (16.2 ± 2.4 GM at 806 nm) was used for the calibration of our measurement technique) . The uncertainty in δ is of the order of 20 %.

EFISHG measurements. The molecular quadratic optical nonlinearities of chromophores, in the form of μgβ products (μg is the ground state permanent dipole moment and β the first hyperpolarizability of the molecules, according to convention B),[58] were measured on a standard Electric Field Induced Second Harmonic Generation (EFISHG) set-up[59] operating at 1907 nm fundamental wavelength, obtained by Raman-shifting the emission from a Nd:YAG laser, and which has the advantage of being far from the absorption bands of the molecules.

DFT calculations. The theoretical absorption spectra have been computed based on Density Functional Theory (DFT) and Time-Dependent DFT (TDDFT). The overall

$$r = \frac{I_{VV} - gI_{VH}}{I_{VV} + 2.g.I_{VH}} \qquad g = \frac{I_{HV}}{I_{HH}}$$

computation strategy was defined as follows: After initial AM1 optimization calculations (vacuum), subsequent optimization of geometrical structures of the derivatives were carried out using the PBE0/6-31G(d) level of calculation. (Note that PBE0 is a good functional for the description of photofunctional molecules).[60] Finally, the TDDFT vertical transitions have

been computed using the same level of calculations. All calculations have been performed using GAUSSIAN 09 package.[61]

diphenyl-4H-pyran-4-yl triphenylphosphonium tetrafluoroborate salt **2**[21] (1 equiv.) in dry THF. After 15 min, the carboxaldehyde (0.9 equiv. and 0.45 in case of compounds **4**) was added. The solution was stirred at -78°C for 30 min, and allowed to warm to room temperature for 2h. THF was evaporated and the residue dissolved in a mixture of CH_2Cl_2/water 1:1 (100 mL) and the organic layer separated. The aqueous layer was extracted with CH_2Cl_2 (2 x 50 mL). The combined organic extracts were dried with $MgSO_4$ and the solvents evaporated.

(E)4-{2-[4-(2,6-Diphenyl-pyran-4-ylidenemethyl)-phenyl]-vinyl}-pyrimidine (3) : Red solid; obtained according to general procedure and purified by column chromatography (SiO_2, CH_2Cl_2/ETA, 1:1) followed by crystallization from $CHCl_3$/n-heptane; yield 65% (277 mg); mp : 227-228 °C (dec); ^{1}H NMR (500 MHz, $CDCl_3$) δ 5.94 (s, 1H), 6.44 (s, 1H), 7.04 (s, 1H), 7.05 (d, 1H, *J* = 16 Hz), 7.31 (d, 1H, *J* = 5Hz), 7.46-7.42 (m, 8H), 7.59 (d, 2H, *J* = 8Hz), 7.78-7.76 (m, 4H), 7.89 (d, 1H, *J* = 16 Hz), 7.66 (d, 1H, *J* = 5 Hz), 9.16 (s, 1H); ^{13}C NMR and JMOD (125 MHz, $CDCl_3$) δ 162.5 (C), 158.9 (CH), 157.3 (CH), 153.3 (C), 151.3 (C), 140.3 (C), 137.3 (CH), 133.4 (C), 133.2 (C), 132.6 (C), 130.5 (C), 129.5 (CH), 129.2 (CH), 128.8 (CH), 128.70 (CH), 128.70 (CH), 128.1 (CH), 125.0 (CH), 124.6 (CH), 124.3 (CH), 118.6 (CH), 113.7 (CH), 108.7 (CH), 102.2 (CH). HRMS (ESI/ASAP) m/z calculated for $C_{30}H_{23}N_2O$ $[M+H]^+$ 427.1810, found 427.1804.

4,6-Bis-{2-[4-(2,6-diphenyl-pyran-4-ylidenemethyl)-phenyl]-vinyl}-pyrimidine (5) : Red solid; obtained according to general procedure and purified by column chromatography (SiO_2, CH_2Cl_2/ETA, 7:3) followed by crystallization from $CHCl_3$/n-heptane; yield 31% (240 mg); mp : 243-244 °C (dec.); ^{1}H NMR (500 MHz, $CDCl_3$) δ 5.95 (s, 2H), 6.45 (s, 2H), 7.06

(s, 2H), 7.08 (d, 2H, *J* = 16 Hz), 7.28 (s, 1H), 7.48-7.40 (m, 16H), 7.61 (d, 4H, *J* = 8Hz), 7.79-7.77 (m, 8H), 7.92 (d, 2H, *J* = 16 Hz), 9.10 (s, 1H); ^{13}C NMR and JMOD (125 MHz, $CDCl_3$) δ 162.9 (C), 158.7 (CH), 153.2 (C), 151.2 (C), 140.1 (C), 136.8 (CH), 133.4 (C), 133.2 (C), 132.8 (C), 130.5 (C), 129.5 (CH), 129.2 (CH), 128.71 (CH), 128.69 (CH), 128.1 (CH), 128.0 (CH), 125.0 (CH), 124.7 (CH), 124.6 (CH), 116.4 (CH), 113.8 (CH), 108.8 (CH), 102.2 (CH). HRMS (ESI) m/z calculated for $C_{56}H_{41}N_2O_2$ $[M+H]^+$ 773.3168, found 773.3163.

Steady-state absorption and fluorescence spectra. The absorption measurements were carried out with a Perkin Elmer Lambda 2 spectrometer. Steady-state fluorescence and phosphorescence spectra were collected from a FluoroMax-4 spectrofluorometer. Emission spectra are spectrally corrected, and fluorescence quantum yields include the correction due to solvent refractive index and were determined relative to quinine bisulfate in 0.05 molar sulfuric acid (Φ_{ref} = 0.52)[51] Due to the very weak emissive chromophores ($\Phi_f < 10^{-3}$), the fluorescence quantum yields were obtained from 5 independent measurements and the uncertainties were determined to ± 20 %. Phosphorescence and steady-state anisotropy measurements were performed in 2-methyl tetrahydrofuran at 77 K. The samples are placed in a 5-mm diameter quartz tube inside a Dewar filled with liquid nitrogen.

Time-gated luminescence. The phosphorescence lifetimes were measured using a FluoroMax-4 spectrofluorometer which is also equipped with a Xe-pulsed lamp operating at up to 25 Hz. The phosphorescence decays are obtained according to a time-gated method. The emission is recorded using a control module that includes a gate-and-delay generator which allows the integration of the signal during a specific period after a flash (delay) and for a pre-determined time window. The total signal is accumulated for a large number of exciting pulses.

Fluorescence anisotropy. For the steady-state anisotropy measurements, two Glan-Thompson polarizers are placed in the excitation and emission beams. The anisotropy r is determined as follows:

Where I is the fluorescence intensity. The subscripts denote the orientation (horizontal H or vertical V) of the excitation and emission polarizers, respectively. g is an instrumental correction factor. The proper calibration of the set-up was checked using a recent standard method with rhodamine 101 in glycerol.[52]

Low-temperature measurements. Low-temperature emission measurements were performed in 2MTHF using a Oxford Cryogenics OptistatDN cryostat fitted with a Oxford Instruments ITC503S temperature controller. The temperature dependency of the refractive index and the density of the solvent were taken into account for the measurement of Φ_f.[53]

Cyclic voltammetry. The cyclic voltammetry experiments[54] (using a computer-controlled Radiometer Voltalab 6 potentiostat with a three-electrode single compartment cell; the working electrode was a platinum disk; a saturated calomel electrode (SCE) used as a reference was placed in a separate compartment with a salt bridge containing the supporting electrolyte) were performed at 300 K, in N_2-degassed dichloromethane with a constant concentration (0.1 M) of n-Bu_4BF_4. Ferrocene (Fc) was used as an internal reference (considering $E_{Fc/Fc+}$ = 0.53 V in CH_2Cl_2 vs. aqueous SCE).[55]

Actinometry. Quantum yields for *trans* → *cis* photoisomerization were measured under irradiation at 436 nm using a 100 W Mercury-Xenon Lamp (Hamamatsu, L2422-02) equipped with a band pass filter (THORLAB, FB430-10). All irradiated solutions were previously N_2-degassed. The progress of the photoreaction was monitored via UV−vis absorption spectra.

The absorbance at excitation wavelength was greater than 2 to assume a total absorption of the incident photons. The incident light intensity was measured by ferrioxalate actinometry.[56]

Open-aperture Z-scan method. The two-photon absorption spectra were measured using open-aperture Z-scan method[30] with a femtosecond mode-locked Ti: Sapphire laser (Coherent, Chameleon Ultra II : pulse duration: 140 ± 20 fs; repetition rate: 80 MHz; wavelength range: 680-1080 nm). After passing through a beam expander (x 4), the laser beam is focused using an f = 15 cm lens and passed through a quartz cell (1 mm optical path length). The position of the sample cell is varied along the laser-beam direction (z-axis) using a Z-step motorized stage controlled by a computer. At constant incident excitation, the local power density within the sample is changed and the corresponding transmitted laser beam, T(z), recorded with a silicon photodetector (Ophir PD300) is monitored in connection with the z-position of the cell. The on-axis peak intensity of the incident pulses at the focal point, I_0, ranged from 30 to 90 GW cm^{-2}. If we assume that the linear absorption of the sample is negligible at working wavelength and that the laser exhibits a Gaussian beam profile in space and time, the nonlinear absorption coefficient β can be calculated from the curve fitting to the experimental transmittance with the following equation:

$$T(z) = 1 - \frac{\beta l I_0}{2\sqrt{2}(1+(\frac{z}{z_0})^2)}$$

Where z_0 is the coordinate along the propagation direction of the focal point of the beam, l the optical path length. The 2PA cross-section, δ, (in units of 1 GM : 10^{-50} cm^4 s photon^{-1} molecule^{-1}) is then determined by using the relationship:

$$\beta = \frac{\delta N_A d}{h\nu} 10^{-3}$$

Where h is the Planck constant, υ the frequency of the incident laser beam, N_A the Avogadro constant and d is the concentration of the chromophore (mol. L^{-1}). The rhodamine 6G in methanol[57] (16.2 ± 2.4 GM at 806 nm) was used for the calibration of our measurement technique) . The uncertainty in δ is of the order of 20 %.

EFISHG measurements. The molecular quadratic optical nonlinearities of chromophores, in the form of μgβ products (μg is the ground state permanent dipole moment and β the first hyperpolarizability of the molecules, according to convention B),[58] were measured on a standard Electric Field Induced Second Harmonic Generation (EFISHG) set-up[59] operating at 1907 nm fundamental wavelength, obtained by Raman-shifting the emission from a Nd:YAG laser, and which has the advantage of being far from the absorption bands of the molecules.

DFT calculations. The theoretical absorption spectra have been computed based on Density Functional Theory (DFT) and Time-Dependent DFT (TDDFT). The overall computation strategy was defined as follows: After initial AM1 optimization calculations (vacuum), subsequent optimization of geometrical structures of the derivatives were carried out using the PBE0/6-31G(d) level of calculation. (Note that PBE0 is a good functional for the description of photofunctional molecules).[60] Finally, the TDDFT vertical transitions have been computed using the same level of calculations. All calculations have been performed using GAUSSIAN 09 package.[61]

Keywords: heterocycle · nonlinear optics · chromophores · pyrimidine · methylenepyran

[1] S. Sumalekshmy, C. Fahrni, C. *J. Chem. Mater.* **2011**, *23*, 483-500.

[2] W. Denk, J. H. Strickler, W. Webb, W. *Science* **1990**, *248*, 73-76.

[3] a) K. J. McEwan, P. A. Fleitz, J. E. Rogers, J. E. Slagle, D. G. McLean, H. Akdas, M. Katterle, I. M. Blake, H. L. Anderson, *Adv. Mater.* **2004**, *16*, 1933-1935. b) Y. Morel, A. Irimia, P. Najechalski, Y. Kervella, O. Stephan, P. L. Baldeck, C. Andraud, *J. Chem. Phys.* **2001**, *114*, 5391-5396. c) J. E. Ehrlich, W. L. Wu, Y. L. Lee, Z. Y. Hu, H. Rockel, S. R. Marder, J. W. Perry, *Opt. Lett.* **1997**, *22*, 1843-1845.

{4] a) C. N. LaFratta, J. T. Fourkas, T. Baldacchini, R. A. Farrer, *Angew. Chem. Int. ed* **2007**, *46*, 6238-6258. b) S. Kawata, H.-B. Sun, T. Tanaka, K. Takada *Nature* **2001**, *412*, 697-698. c) Sun, H.-B.; Kawata, S. *Two-Photon Photopolymerization and 3D Lithographic Microfabrication*; Springer-Verlag ed. Berlin, 2004; Vol. 170. d) M. Jin, J. P. Malval, D. L. Versace, F. Morlet-Savary, H. Chaumeil, A. Defoin, X. Allonas, J. P. Fouassier, *Chem. Comm.* **2008**, *48*, 6540-6542. e) J. P. Malval, M. Jin, F. Morlet-Savary, H. Chaumeil, A. Defoin, O. Soppera, T. Scheul, M. Bouriau, P. L. Baldeck, *Chem. Mater.* **2011**, *23*, 3411-3420. f) J. P. Malval, F. Morlet-Savary, H. Chaumeil, L. Balan, D.-L. Versace, M. Jin, A. Defoin, *J. Phys. Chem. C* **2009**, *113*, 20812-20821. g) R. Xia, J. P. Malval, M. Jin, A. Spangenberg, D. Wan, H. Pu, T. Vergote, F. Morlet-Savary, H. Chaumeil, P. Baldeck, O. Poizat, O. Soppera, *Chem. Mater.* **2012**, *24*, 237-244.

{5] a) W. H. Zhou, S. M. Kuebler, K. L. Braun, T. Y. Yu, J. K. Cammack, C. K. Ober, J. W. Perry, S. R. Marder, *Science* **2002**, *296*, 1106-1109. b) B. H. Cumpston, S. P. Ananthavel, S. Barlow, D. L. Dyer, J. E. Ehrlich, L. L. Erskine, A. A.; Heika, S. M. Kuebler, I.-Y. S. M.; Lee, D. McCord-Maughon, J. Qin, H. Röckel, M. Rumi, X.-L. Wu, S. R. Marder, J. W. Perry, *Nature* **1999**, *398*, 51-54.

{6] a) G. S. He, L.-S. Tan, Q. Zheng, P. N. Prasad, *Chem. Rev.* **2008**, *108*, 1245-1330. b) M. Pawlicki, H. A. Collins, R. G. Denning, H. L. Anderson, *Angew. Chem. Int. ed* **2009**, *48*, 3244-3266.

[7] A. Bhaskar, G. Ramakrishna, Z. Lu, R. Twieg, J. M. Hales, D. J. Hagan, E. V. Stryland, T. Goodson, *J. Am. Chem. Soc.* **2006**, *128*, 11840-11849.

[8] a) M. G. Kuzyk, *J. Chem. Phys.* **2003**, *119*, 8327-8334. b) J. P. Moreno, M. G. Kuzyk,. J. Chem. Phys. **2005**, *123*, 194101.

[9] a) M. Johnsen, M. J. Paterson, J. Arnbjerg, O. Christiansen, C. B. Nielsen, M. Jorgensen, P. R. Ogilby, *Phys. Chem. Chem. Phys.* **2008**, *10*, 1177-1191. b) M. Rumi, J. E. Ehrlich, A. Heikal, J. W. Perry, S. Barlow, Z. Y. Hu, D. McCord-Maughon, T. C. Parker, H. Rockel, S. Thayumanavan, S. R. Marder, D. Beljonne, J. L. Brédas,. *J. Am. Chem. Soc.* **2000**, *122*, 9500-9510.

[10] a) K. D. Belfield, M. V. Bondar, F. E. Hernandez, O. V. Przhonska, S. Yao, *J. Phys. Chem. B* **2007**, *111*, 12723-12729. b) K. D. Belfield, A. R. Morales, B.-S. Kang, J. M. Hales, D. J. Hagan, E. W. V. Stryland, V. M. Chapela, J. Percino, *Chem. Mater.* **2004**, *16*, 4634-4641. c) K. D. Belfield, K. J. Schafer, W. Mourad, B. A. Reinhardt, *J. Org. Chem.* **2000**, *65*, 4475-4481.

[11] O. K. Kim, K. S. Lee, Z. Huang, W. B. Heuer, C. S. Paik-Sung, *Opt. Mater.* **2003**, *21*, 559-564.

[12] a) T. K. Ahn, K. S. Kim, D. Y. Kim, S. B. Noh, N. Aratani, C. Ikeda, A. Osuka, D. Kim, D. *J. Am. Chem. Soc.* **2006**, *128*, 1700-1704. b) M.-C. Yoon, S. B.; Noh, A. Tsuda, Y. Nakamura, A. Osuka, D. Kim, *J. Am. Chem. Soc.* **2007**, *129*, 10080-10081. c) S. Drouet, A. Merhi, D. D. Yao, M. P. Cifuentes, M. G. Humphrey, M. Wielgus, J. Olesiak-Banska, K. Matczyszyn, M. Samoc, F. Paul, C. O. Paul-Roth *Tetrahedron* **2012**, *68*, 10351-10359.

[13] a) D. Beljonne, W. Wenseleers, E. Zojer, Z. Shuai, H. Vogel, S. J. K. Pond, J. W. Perry, S. R. Marder, J. L. Brédas, *Adv. Funct. Mater.* **2002**, *12*, 631-641. b) C. K. M. Chan, C.

H. Tao, K.-F. Li, K. M. C. Wong, N. Y. Zhu, K.-W. Cheah, V. W.-W. Yam, *Dalton Trans.* **2011**, *40*, 10670-10685.

[14] a) S. J. K. Pond, O. Tsutsumi, M. Rumi, O. Kwon, E. Zojer, J. L. Brédas, S. R. Marder, J. W. Perry, *J. Am. Chem. Soc.* **2004**, *126*, 9291-9306. b) S. J. Chung, M. Rumi, V. Alain, S. Barlow, J. W. Perry, S. R. Marder, *J. Am. Chem. Soc.* **2005**, *127*, 10844-10845. c) C. Katan, S. Tretiak, M. H. V. Werts, A. J. Bain, R. J. Marsh, N. Leonczek, N. Nicolaou, E. Badaeva, O. Mongin, M. Blanchard-Desce, *J. Phys. Chem. B* **2007**, *111*, 9468-9483. d) C. Katan, F. Terenziani, O. Mongin, M. H. V. Werts, L. Porrès, T. Pons, J. Mertz, S. Tretiak, M. Blanchard-Desce, *J. Phys. Chem. A* **2005**, *109*, 3024-3037.

[15] a) C. Katan, S. Tretiak, J. Even, *Proc. SPIE* **2010**, *7712*, 77123D. b) H. Akdas-Kilig, J. P. Malval, F. Morlet-Savary, A. Singh, L. Toupet, I. Ledoux-Rak, J. Zyss, H. Le Bozec, H. *Dyes Pigm.* **2012**, *92*, 681-688.

[16] a) A. Adronov, J. M. J. Fréchet, G. S. He, K.-S. Kim, S.-J. Chung, J. Swiatkiewicz, P. N. Prasad, *Chem. Mater.* **2000**, *12*, 2838-2841. b) M. Drobizhev, A. Karotki, Y. Dzenis, A. Rebane, Z. Suo, C. W. Spangler, *J. Phys. Chem. B* **2003**, *107*, 7540-7543. c) A. Abbotto, L. Beverina, R. Bozio, A. Facchetti, C. Ferrante, G. A. Pagani, D. Pedron, R. Signorini, *Chem. Commun.* **2003**, 2144-2145. d) K. A. Green, M. P. Cifuentes, M. Samoc, M. G. Humphrey, *Coord. Chem. Rev.* **2011**, *255*, 2025-2038.

[17] a) S. Achelle, N. Plé, *Curr. Org. Synth.* **2012**, *9*, 163-187. b) S. Achelle, A. Barsella, C. Baudequin, B. Caro, F. Robin-le Guen, *J. Org. Chem.* **2012**, *77*, 4087-4096. c) S. Achelle, N. Saettel, P. Baldeck, M. P. Teulade-Fichou, P. Maillard, *J. Porphyrins Phtalocyanines* **2010**, *14*, 877-884.

[18] a) N. Faux, F. Robin-le Guen, P. le Poul, B. Caro, K. Nakatani, E. Ishow, S. Golhen, *Eur. J. Inorg. Chem.* **2006**, 3489-3497. b) R. Andreu, L. Carrasquer, S. Franco, J. Garin, J. Orduna, N. Martinez de Baroja, R. Alicante, B. Villacampa, M. Allain, M. *J. Org. Chem.* **2009**, *74*, 6647-6657. c) R. Andreu, E. Galan, J. Garin, V. Herrero, E. Lacarra, J. Orduna, R. Alicante, B. Villacampa, *J. Org. Chem.* **2010**, *75*, 1684-1692. d) R. Andreu, E. Galán, J. Orduna, B. Villacampa, R. Alicante, J. T. López Navarrete, J. Casado, J. Garín, *Chem. Eur. J.* **2011**, *17*, 826-838.

[19] a) S. R. Marder, D. N. Beratan, L.-T. Cheng, *Science* **1991**, *252*, 103-106. b) G. Bourhill, J. L. Bredas, L.-T. Cheng, S.R. Marder, F. Meyers, J. W. Perry, B. G. Tiemann, *J. Am. Chem. Soc.* **1994**, *116*, 2619-2620. c) I. D. L. Albert, T. J. Marks, M. A. Ratner, *J. Am. Chem. Soc.* **1997**, *119*, 3155-3156.

[20] a) J.-J. Vanden Eynde, L. Pascal, Y. Van Haverbeke, P. Dubois, *Synth. Commun.* **2001**, *31*, 3167-3173. b) L. Pascal, J. J.; Vanden Eynde, Y. Van Haverbeke, P. Dubois, A. Michel, U. Rant, E. Zojer, G. Leising, L. O. Van Dorn, N. E. Gruhn, J. Cornil, J. L. Brédas, *J. Phys. Chem. B* **2002**, *106*, 6442-6450.

[21] C. H. Chen, G. A. Reynolds, *J. Org. Chem.* **1980**, *45*, 2453-2458.

[22] F. Ba, F. Robin-Le Guen, N. Cabon, P. Le Poul, S. Golhen, N. Le Poul, B. Caro, *J. Organomet. Chem.* **2010**, *695*, 235-243.

[23] J. R. Platt, *J. Chem. Phys.* **1949**, *17*, 484-495.

[24] F. Ba, N. Cabon, F. Robin-Le Guen, P. Le Poul, N. Le Poul, Y. Le Mest, S. Golhen, B. Caro, *Organometallics* **2008**, *27*, 6396-6399.

[25] F. Ba, N. Cabon, P. le Poul, S. Kahlal, J.-Y. Saillard, N. le Poul, S. Golhen, B. Caro, F. Robin-le Guen, *New J. Chem.* **2013**, *doi : 10.1039/C3NJ41126E*

[26] K. Itami, D. Yamazaki, J. Yoshida, *J. Am. Chem. Soc.* **2004**, *126*, 15396-15397.

[27] S. Dufresne, G. S. Hanan, W. G. Skene, *J. Phys. Chem. B* **2007**, *111*, 11407-11418.

[28] Davidov, A. S. *Theory of molecular excitons;* Plenum Press: New York, 1971.

[29] F. Terenziani, C. Katan, E. Badaeva, S. Tretiak, M. Blanchard-Desce, *Adv. Mater.* **2008**, *20*, 4641-4678.

[30] a) M. Sheik-Bahae A. A. Said, E. W. V. Stryland, Opt. Lett. **1989**, *14*, 955-957. b) M. Sheik-Bahae; A. A. Said, T. H. Wei, D. J. Hagan, E. W. V. Stryland, *IEEE J. Quant. Electron.* **1990**, *26*, 760-769.

[31] a) J. P. Malval, J. P. Morand, R. Lapouyade, W. Rettig, G. Jonusauskas, J. Oberle, C. Trieflinger, J. Daub, *Photochem. Photobiol. Sci.* **2004**, *3*, 939-948. b) D. Rehm, A. Weller, *Isr. J. Chem.* **1970**, *8*, 259.

[32] L. Antonov, K. Kamada, K. Ohta, F. S. Kamounah, *Phys. Chem. Chem. Phys.* **2003**, *5*, 1193-1197.

[33] J.-P. Malval, F. Morlet-Savary, H. Chaumeil, L. Balan, D.-L. Versace, M. Jin, A. Defoin,. *J. Phys. Chem. C* **2009**, *113*, 20812-20821.

[34] Y.-Z. Cui, Q. Fang, G. Xue, G.-B. Xu, L. Yin, W.-T. Yu, *Chem. Phys.* **2005**, *34*, 644-645.

[35] a) K. D. Singer, A. F. Garito, *J. Phys. Chem.* **1981**, *75*, 3572-3580. b) B. F. Levine, C. G. Bethea, *Appl. Phys. Lett.* **1974**, *24*, 445-447. c) I. Ledoux, J. Zyss, Chem. Phys. **1982**, *73*, 203-213.

[36] a) E. Z. Lippert, *Naturforsch.* **1955**, *10a*, 541-545. b) N. Mataga, Y. Kaifu, M. Koizumi, *Bull. Chem. Soc. Jpn.* **1955**, *28*, 690-691.

[37] a) W. Verbouwe, M. Van der Auweraer, F. C. De Schryver, J. J. Piet, J. M. Warman, *J. Am. Chem. Soc.* **1998**, *120*, 1319-1324. b) W. Verbouwe, L. Viaene, M. Van der Auweraer, F. C. De Schryver, H. Masuhara, R. Pansu, J. Faure, *J. Phys. Chem. A* **1997**, *101*, 8157-8165.

[38] a) N. P. Ernsting, J. Breffke, D. Y. Vorobyev, D. A. Duncan, I. Pfeffer, *Phys. Chem. Chem. Phys.* **2008**, *10*, 2043-2049. b) J. F. Letard, R. Lapouyade, W. Rettig, *J. Am. Chem. Soc.* **1993**, *115*, 2441-2447. c) R. Lapouyade, K. Czeschka, W. Majenz, W. Rettig, E. Gilabert, C. Rulliere, *J. Phys. Chem.* **1992**, *96*, 9643-9650. d) Y. V. Il'ichev, W. Kuhnle, K. A. Zachariasse, *Chem. Phys.* **1996**, *211*, 441-453.

[39] H. Gruen, H. Görner, *J. Phys. Chem.* **1989**, *93*, 7144-7152.

[40] a) D. H. Waldeck, *Chem. Rev.* **1991**, *91*, 415-436. b) J. Saltiel, A. S. Waller, D. F. Sears, E. A. Hoburg, D. M. Zeglinski, D. H. Waldeck, *J. Phys. Chem.* **1994**, *98*, 10689-10698.

[41] a) H. Görner, *J. Photochem. Photobiol., A* **1987**, *40*, 325-339. b) H. Görner, D. Schulte-Frohlinde, *J. Photochem.* **1978**, *8*, 91-102. c) V. Papper, D. Pines, G. Likhtenshtein, E. Pines, *J. Photochem. Photobiol., A* **1997**, *111*, 87-96.

[42] a) J. Saltiel, A. Marinari, D. W. L. Chang, J. C. Mitchener, E. D. Megarity, *J. Am. Chem. Soc.* **1979**, *101*, 2982-2996. b) H. Görner, D. Schulte-Frohlinde, *J. Phys. Chem.* **1978**, *82*, 2653-2659.

[43] a) P. J. Suppan, *Photochem. Photobiol., A* **1990**, *50*, 293-330. b) T. Hagan, D. Pilloud, P. Suppan, *Chem. Phys. Lett.* **1987**, *139*, 499-502.

[44] a) T. Furutsuka, T. Imura, T. Kojima, K. Kawabe, *Techn. Rep. Osoka Univ.* **1974**, 367. b) A. C. Ling, J. E. Willard, *J. Phys. Chem.* **1968**, *72*, 1918-1923.

[45] a) G. U. Bublitz, S. G. Boxer, *J. Am. Chem. Soc.* **1998**, *120*, 3988-3992. b) M. Goes, M. de Groot, M. Koeberg, J. W. Verhoeven, N. R. Lokan, M. J.; Shephard, M. N. Paddon-Row, *J. Phys. Chem. A* **2002**, *106*, 2129-2134.

[46] Z. R. Grabowski, K. Rotkiewicz, W. Rettig, *Chem. Rev.* **2003**, *103*, 3899-4032.

[47] a) H. El-Gezawy, W. Rettig, R. Lapouyade, *J. Phys. Chem. A* **2005**, *110*, 67-75. b) R. Lapouyade, A. Kuhn, J. F. Letard, W. Rettig, *Chem. Phys. Lett.* **1993**, *208*, 48-58. c) W. Rettig, W. Majenz, R. Herter, J.-F. Létard, R. Lapouyade, *Pure Appl. Chem.* **1983**, *65*, 1699-1704. d) E. Abraham, J. Oberlé, G. Jonusauskas, R. Lapouyade, C. Rullière, *J. Photochem. Photobio., A* **1997**, *105*, 101-107. e) J.-F. Letard, R. Lapouyade, W. Rettig, *Chem. Phys.* **1994**, *186*, 119-131. f) E. Abraham, J. Oberlé, G. Jonusauskas, R. Lapouyade, C. Rullière, *Chem. Phys.* **1997**, *214*, 409-423.

[48] a) J.-S. Yang, K.-L. Liau, C.-M. Wang, C.-Y. Hwang, *J. Am. Chem. Soc.* **2004**, *126*, 12325-12335. b) F. D. Lewis, W. Weigel, *J. Phys. Chem. A* **2000**, *104*, 8146-8153. c) F. D. Lewis, W. Weigel, X. Zuo, *J. Phys. Chem. A* **2001**, *105*, 4691-4696. d) F. D. Lewis, R. S. Kalgutkar, J.-S. Yang, *J. Am. Chem. Soc.* **1999**, *121*, 12045-12053.

[49] C.-C. Cheng, W.-S. Yu, P.-T. Chou, S.-M. Peng, G.-H. Lee, P.-C. Wu, Y.-H. Song, Y. Chi, *Chem. Commun.* **2003**, 2628-2629.

[50] a) J.-S. Yang, S.-Y. Chiou, K.-L. Liau, *J. Am. Chem. Soc.* **2002**, *124*, 2518-2527. b) J.-Y. Yang, K.-L. Liau, C.-Y. Hwang, C.-M. Wang, C *J. Phys. Chem. A* **2006**, *110*, 8003-8010. c) J.-Y.Yang, C.-K. Lin, A. M. Lahoti, C.-K. Tseng, Y.-H. Liu, G.-H. Lee, S.-M. Peng, *J.*

Phys. Chem. A **2009**, *113*, 4868-4877. d) J.-S. Yang, K.-L. Liau, C.-Y. Li, M.-Y. Chen, *J. Am. Chem. Soc.* **2007**, *129*, 13183-13192.

[51] R. Meech, D. Phillips, *J. Photochem.* **1983**, *23*, 193–217.

[52] T. J. V. Prazeres, A. Fedorov, S. P. Barbosa, J. M. G. Martinho, M. N. Berberan-Santos, *J. Phys. Chem. A* **2008**, *112*, 5034–5039.

[53] T. Rong-Ri, S. Xin, H. Lin, Z. Feng-Shou, *Chin. Phys. B* **2012**, *21*, 086402.

[54] J.-P. Malval, C. Chaimbault, B. Fischer, J.-P. Morand, R. Lapouyade, *Res. Chem. Intermed.* **2001**, *27*, 21-34.

[55] P. Hapiot, L. D. Kispert, V. V. Konovalov, J.-M.; Savéant, *J. Am. Chem. Soc*. **2001**, *123*, 6669-6677.

[56] M. Montalti, A. Credi, L. Prodi, M. T. Gandolfi, Handbook of Photochemistry, Third Ed.; CRC Press: Boca Raton, 2006.

[57] P. Sengupta, J. Balaji, S. Banerjee, R. Philip, G. R. Kumar, S. Maiti, *J. Chem. Phys.* **2000**, *112*, 9201-9205.

[58] a) A. Willetts, J. E. Rice, D. M.; Burland, *J. Chem. Phys.* **1992**, *97*, 7590-7599. b) H. Reis, *J. Chem. Phys.* **2006**, *125*, 014506.

[59] T. Thami, P. Bassoul, M. A. Petit, J. Simon, A. Fort, M. Barzoukas, A. Villayes, *J. Am. Chem. Soc.* **1992**, *114*, 915-921.

[60] S. Aloise, Z. Pawlowska, C. Ruckebusch, M. Sliwa, J. Dubois, O. Poizat, G. Buntinx, A. Perrier, F. Maurel, P. Jacques, J.-P. Malval, L. Poisson, G. Piani, J. Abe, *Phys. Chem. Chem. Phys.* **2012**, *14*, 1945-1956.

[61] Frisch, M. J. In *Gaussian 09, Revision B.01, Gaussian, Inc., Wallingford CT* Wallingford CT, 2009.

TOC

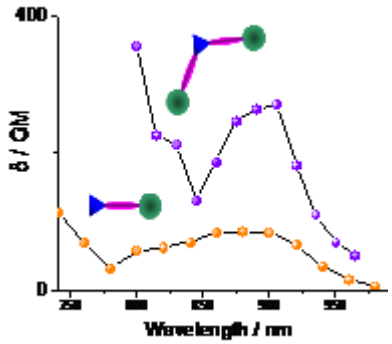

The nonlinear properties and the photophysical behavior of a series of π-conjugated chromophores incorporating an electron-deficient pyrimidine core (A) and γ-methylenepyrans as terminal donor (D) groups have been thoroughly investigated.